Evidence of centromeric histone 3 chaperone involved in DNA damage repair pathway

Authors: Prakhar Agarwal and Santanu Kumar Ghosh*

Affiliation: Department of Biosciences and Bioengineering, Indian Institute of Technology, Bombay, Powai, Mumbai-400076, India.

*Corresponding author

Email: santanughosh@iitb.ac.in

Tel. +(91-22) 2576 7766

Fax. (+91)22 2572 3480

Key words: Scm3, HJURP, DNA damage, centromere, chromosome, budding yeast

Abstract

The centromeric protein-A (CENP-A) is an evolutionary conserved histone H3 variant that marks the identity of the centromeres. Several mechanisms regulate the centromeric deposition of CENP-A as its mislocalization causes erroneous chromosome segregation, leading to aneuploidy-based diseases, including cancers. The most crucial deposition factor is a CENP-A specific chaperone, HJURP (Scm3 in budding yeast), which specifically binds to CENP-A. However, the discovery of HJURP as a DDR (DNA damage repair) protein and evidence of its binding to Holliday junctions in vitro indicate a CENP-A-deposition-independent role of these chaperones. In this study, using budding yeast, we demonstrate that Scm3 is crucial for the DDR pathway as *scm3* cells are sensitive to DNA damage. We further observe that the *scm3* mutant interacts with the *rad52* DDR mutant and is compromised in activating DDR-mediated arrest. We demonstrate that Scm3 associates with the DNA damage sites and undergoes posttranslational modifications upon DNA damage. Overall, from this report and earlier studies on HJURP, we conclude that DDR functions of CENP-A chaperones are conserved across eukaryotes. Thus, the revelation that these chaperones confer genome stability in more than one pathway has clinical significance.

Introduction

The faithful replication and partitioning of the replicated chromatin as chromosomal units from mother to daughter cell is important for cell survival. New nucleosomes, the units of chromatin, are assembled on DNA during replication that requires deposition of the histones within the nucleosomes in a highly regulated step-by-step process that involves the deposition of $(H3\text{-}H4)_2$ tetramer followed by two H2A-H2B dimers (Hammond et al., 2017; Ransom et al., 2010). The deposition of the histones to their specific positions within the nucleosome occurs in a temporal manner assisted by a group of proteins called histone chaperones. For this, the chaperones physically interact with the histones in a pre-nucleosomal complex and thus prevent premature histone-DNA interaction or nucleosome assembly (Burgess and Zhang, 2013; Ransom et al., 2010). The deposition of the canonical histones at the gross chromatin takes place mostly during DNA replication via a replication-coupled (RC) pathway using the chaperones dedicated to the RC pathway (Serra-Cardona & Zhang, 2018). For instance, Asf1 and CAF-1 deposit $(H3\text{-}H4)_2$ tetramer (Burgess and Zhang, 2013; De Koning et al., 2007) and Nap1 facilitates $(H2A\text{-}H2B)_2$ assembly (De Koning et al., 2007; Eitoku et al., 2008) into the nucleosomes. On the other hand, the variant histones that earmark specialized chromatin domains committed to do specific biological functions are deposited at specific sites throughout the cell cycle using replication-independent (RI) pathway using variant-specific chaperones dedicated to RI pathway (Smith, 2002). For Instance, deposition of the variant histones H2A.Z, centromeric H3 (CenH3), MacroH2A signifying transcriptional activation (Giaimo et al., 2019), kinetochore formation (Earnshaw and Rothfield, 1985; Earnshaw and Tomkiel, 1992; McKinley and Cheeseman, 2016) and X chromosome inactivation (Sun and Bernstein, 2019) occurs via chromatin remodeler (Fan et al., 2022), HJURP chaperone (Dunleavy et al., 2009; Foltz et al., 2009) and acidic nuclear phosphoprotein 32B (ANP32B) (Mandemaker et al., 2023), respectively.

Almost all the eukaryotes harbor CenH3 at the centromeres, which promotes the formation of kinetochore at those loci (Blower and Karpen, 2001; Buchwitz et al., 1999; Howman et al., 2000; Stoler et al., 1995; Van Hooser et al., 2001). Since the kinetochores bind to the microtubules and drive faithful chromosome segregation, deposition of CenH3 at the centromeres is essential for cell survival. In metazoans, CENP-A (Centromeric protein- A) is the CenH3 (Earnshaw and Rothfield, 1985), and HJURP (Holliday junction recognition protein) is the cognate chaperone (Dunleavy et al., 2009; Foltz et al., 2006). The CENP-A binding domain within HJURP present at its N-terminal is highly conserved (Aravind et al., 2007; Sanchez-Pulido et al., 2009; Shuaib et al., 2010). Despite the well-established function of HJURP in CENP-A deposition at the centromeres, HJURP was initially identified as a

protein involved in DNA damage response (DDR) due to the following reasons (Kato et al., 2007). HJURP was so named because of its ability to bind in vitro to Holliday junction DNA substrates that are in vivo generated during DNA damage repair through homologous recombination. In addition, HJURP was found to interact physically with DNA damage sensing complex MRN (Mre11-Rad50-Nbs1), and the interaction was found to increase significantly upon induction of double-strand breaks (DSBs). As a corollary, the level and subcellular localization of HJURP change in the cells treated with DNA-damaging agents such as Infrared Radiation (IR), Hydroxyurea (HU), cisplatin, and camptothecin (CPT). Finally, the expression of HJURP was found to be regulated by ATM, a DDR kinase, as no expression was observed in ATM-deficient cancerous cell lines. Perhaps due to genome wide function on DDR, HJURP has been visualized to be diffusely present throughout the nucleus (Dunleavy et al., 2009; Kato et al., 2007).

Given the functions of HJURP in CENP-A deposition and DDR pathway, it is not surprising that misregulation of HJURP is involved in disease states. HJURP is considered an oncogene as its overexpression has been associated with several cancers (Chen et al., 2018; Kang et al., 2020) including breast cancer (Coates et al., 2010; Hu et al., 2010; Montes de Oca et al., 2015), lung cancer (Kato et al., 2007), ovarian cancer (Dou et al., 2022), glioblastoma (Valente et al., 2013, 2009), hepatocellular carcinoma (Chen et al., 2018; Hu et al., 2017; Luo et al., 2022), colorectal cancer (Kang et al., 2020) and in pancreatic cancer (Wang et al., 2020). Consequently, the inhibition of HJURP attenuates the properties of the cancer cells and increases the survival rate of the patients, and thus, HJURP acts as a prognostic marker for several cancers (Kang et al., 2020; Lai et al., 2021).

In budding yeast, Cse4 and Scm3 are the homologs of CENP-A and HJURP, respectively. Scm3 deposits Cse4 at the centromeres during the S phase through its physical interaction with Ndc10 that binds to the centromeric DNA as a part of the CBF3 complex (Camahort et al., 2007; Cho and Harrison, 2012, 2011). It has been shown that following the deposition of Cse4, Scm3 remains associated with the centromeres throughout the cell cycle (Wisniewski et al., 2014; Xiao et al., 2011). Like HJURP, Scm3 has been found on the gross chromatin besides its localization at the centromeres (Mizuguchi et al., 2007). Furthermore, a comparison of the domain organization between HJURP and Scm3 suggests that besides the highly conserved CENP-A binding domain, both HJURP and Scm3 also harbour homologous DNA binding domain (Figure S1), which is predicted to be evolutionarily conserved in all vertebrates and fission yeast (Müller et al., 2014). Notably, overexpressed Scm3, like HJURP, shows chromosome instability, and it is believed that Scm3, when excess, binds to the centromeric DNA independently and leads to chromosome missegregation (Choy et al., 2012;

103 Mishra et al., 2011). Both the proteins dimerizes and in *in-vitro* assay, they can bind even to
104 non-*CEN* DNA (Kato et al., 2007; Xiao et al., 2011). While there is no mammalian homolog of
105 budding yeast Ndc10 and no yeast homolog of mammalian Mis18, both these proteins are
106 critical for CENP-A deposition as they bind to their respective CENP-A chaperones through
107 regions independent of CENP-A or DNA binding domain. Therefore, despite the large
108 difference in the polypeptide length between HJURP and Scm3 (748 vs. 229), most of the
109 functions are highly conserved from humans to yeast. Given the physical interaction of HJURP
110 with the MRN complex, it is highly plausible that Scm3 might also interact with DDR proteins
111 in yeast. Altogether, from the above observations, we hypothesize that Scm3, like HJURP,
112 may also be involved in the DDR pathway in budding yeast. In this work, we report that the
113 cells lacking Scm3 are sensitive to the DNA damaging agents and are compromised both in
114 DNA damage repair. In addition to the known functions of HJURP in DDR pathway, in this
115 report we show, using Scm3, that these chaperones are required for mounting DDR-
116 dependent checkpoint activation. Importantly, we demonstrate for the first time that they
117 indeed associate with the DNA damage sites upon induction of DNA damage and persists
118 there perhaps to facilitate damage repair. Our results suggest that the phosphorylation of
119 Scm3 may be attributed to the DDR functions of Scm3. Taken together, this study reveals an
120 evolutionary kinship amongst CenH3 chaperones in conferring genome stability through
121 efficient DNA damage repair, besides their canonical role in CenH3 deposition.

122 **Results**

123 **Scm3 depleted cells are sensitive to MMS mediated DNA damage.**
124 The yeast cells compromised in DNA damage repair (DDR) function show sensitivity to DNA
125 damaging agents such as methyl methane sulfonate (MMS), HU and CPT. To investigate the
126 role of Scm3 in DDR, we constructed an auxin-inducible (Nishimura et al., 2009) Scm3
127 conditional mutant since the protein is essential for growth (Camahort et al., 2007; Mizuguchi
128 et al., 2007; Stoler et al., 2007), and assayed the behaviour of the mutant in the presence of
129 the DNA damaging agents. Since the cells devoid of the homologous recombination protein,
130 Rad52, are known to show extreme sensitivity to such drugs, *rad52*Δ cells were taken as a
131 positive control in our assays (Hallwyl et al., 2008; Kaytor and Livingston, 1994). Mid-log grown
132 cells were harvested, serially diluted, and spotted on plates supplemented with auxin and DNA
133 damaging agents (MMS, HU, CPT) in different combinations and found similar results for all
134 the drugs (Figure 1A, Figure S2A). We observed that *scm3* mutants (three independent
135 transformants) were more sensitive in the presence of MMS (plate supplemented with both
136 auxin and MMS) as compared to those without MMS (plate supplemented with only auxin),
137 whereas *rad52*Δ cells, as expected, were sensitive to MMS but not to auxin (Figure 1A). To

138 quantify the levels of sensitivity towards MMS, we performed a CFU count assay where *SCM3-*
139 *AID* cells were pregrown in rich media without auxin till the mid-log phase before an equal
140 number of cells were plated on media supplemented with auxin and MMS in different
141 combinations as indicated in Figure 1A. The number of colonies formed after 36 hrs were
142 counted and are quantified as follows. The number of colonies that appeared on the plates
143 free of auxin and MMS were taken as 100% cell viability; with respect to this, the number of
144 colonies that appeared on other plates (conditions) was used to calculate the viability
145 percentage for those conditions. We observed a statistically significant drop in cell viability in
146 the plate supplemented with both auxin and MMS compared to auxin alone (Figure 1B).
147 Since the presence of auxin in the plate can hinder the growth of the *SCM3-AID* cells,
148 in another approach to examine the sensitivity of *scm3* mutant to MMS, we pre-treated the
149 cells with 0.75 mM auxin for 2 hrs to deplete Scm3 before they were washed and spotted on
150 plates containing different concentrations of MMS, but without auxin. The depletion of Scm3
151 was verified by observing higher percentage of G2/M arrested cells (Figure S2B). Here also
152 we found that Scm3-depleted cells were more sensitive to MMS as compared to the wild-type
153 cells (Figure S2C). To quantify the sensitivity observed by this approach, we performed a CFU
154 count assay as above. Following auxin pretreatment, an equal number of wild-type, *SCM3-*
155 *AID,* and *rad52*Δ cells were spread on the YPD plate or YPD plate containing 0.01% MMS. By
156 calculating the viability percentage as described above, we again found a statistically
157 significant drop in cell viability on the plate where Scm3 was predepleted (Figure S2D). The
158 *rad52*Δ cells, as the positive control, showed high sensitivity, as expected.
159 The increased sensitivity of *scm3*-depleted cells to DNA-damaging agents could be
160 due to weakening of the kinetochores as Scm3-mediated deposition of Cse4 promotes
161 kinetochore assembly (Camahort et al., 2007; Cho and Harrison, 2011). If this holds true,
162 perturbation of the kinetochore by degradation of other kinetochore proteins must show a
163 similar sensitivity to MMS. In budding yeast, Ndc10 is recruited to the centromeres upstream
164 of Scm3 (Lang et al., 2018), whereas the centromeric localization of Mif2, another essential
165 inner kinetochore protein, depends on Scm3 and Cse4 (Xiao et al., 2017). We constructed
166 *NDC10-AID* and *MIF2-AID* strains and used them for our assay to represent the proteins
167 independent or dependent on Scm3 for centromeric localization, respectively. We also
168 included one non-essential kinetochore protein, Ctf19, a protein of the COMA complex, to
169 remove any possible mis-judgement in distinguishing cell-growth-arrest phenotype occurring
170 due to drug-sensitivity vs. auxin-mediated degradation of essential proteins. The COMA
171 complex is directly recruited to the centromeres through interaction with the N terminal tail of
172 Cse4, hence dependent on Scm3 (Chen et al., 2000; Fischböck-Halwachs et al., 2019). Mid-
173 log grown cells were harvested and spotted on the indicated plates, however, we did not
174 observe any increased sensitivity of such cells to MMS (Figure S3). In fact, Mif2 depleted cells

175 showed a slight resistance to MMS due to unknown reasons. Therefore, the increased
176 sensitivity to MMS in *scm3* mutant but not in other kinetochore mutant cells indicates that
177 Scm3 possesses an additional function in genome stability besides its role in kinetochore
178 assembly.

179 Since HJURP is involved in DDR through the HR pathway (Kato et al., 2007) and If
180 Scm3 mimics HJURP to repair damaged DNA, then the *scm3* mutant is expected to interact
181 genetically with the HR mutants. We tested that possibility by analyzing the genetic interaction
182 between *SCM3* and *RAD52,* as Rad52 is essential for efficient homologous recombination in
183 *S. cerevisiae* (Barlow & Rothstein, 2010; Lee et al., 2003). We deleted *RAD52* in the *SCM3-*
184 *AID* strain, and the mid-log grown cells were spotted on plates supplemented with increasing
185 concentrations of auxin (Figure 1C). Interestingly, the double mutant grew slowly as compared
186 to the single mutants and the wild-type strain. To further validate the genetic interaction
187 between the two genes, the mid-log grown cells were pre-treated with a 0.75 mM auxin to
188 deplete Scm3 for the indicated duration before the cells were spotted on YPD plates. Again,
189 we observed that the double mutant grew slower than the wild-type and single mutants (Figure
190 1D). Next, we wished to investigate how the double mutant behaves when challenged with
191 DNA damaging agent. As expected, when the double mutant was spotted in the presence of
192 0.005% MMS, all the single mutants grew better than the double mutant (Figure S2E). These
193 results indicate a genetic interaction between *SCM3* and *RAD52,* which becomes pronounced
194 in the presence of DNA-damaging agents.

195 Further, we wanted to identify the regions in Scm3 whose loss confers sensitivity to
196 DNA damage. The domain organization of Scm3 reveals two essential conserved regions,
197 namely NES (nuclear export signal) and HR (heptad repeat), having functions in DNA and
198 Cse4 binding, respectively (Figure S1A). Scm3 has a non-essential D/E-rich region, which is
199 important for protein stability but not involved in Cse4 binding (Stoler et al., 2007). Scm3 also
200 possesses two BR (bromodomain) regions, also referred to as the NLS (nuclear localization
201 signal). The deletion of the C-terminal 25 amino acids or the bromodomain regions does not
202 cause cell lethality (Shivaraju et al., 2011; Stoler et al., 2007). We used the versions of Scm3
203 mutants used elsewhere (Shivaraju et al., 2011) harbouring deletion in one or the other non-
204 essential region as the sole source of Scm3 and challenged these mutants (two independent
205 transformants) to MMS and CPT along with wild-type Scm3 as a control. We found no growth
206 defect in response to MMS or CPT (Figure S1B) suggesting that at least the nonessential
207 regions are not important for the DDR function of Scm3. Although this indicates that the
208 essential NES and/or HR might be involved but that is technically difficult to test using growth
209 based assays.

210 From these results, we conclude that the loss of Scm3 confers sensitivity to DNA
211 damaging agents, indicating that Scm3, much like its mammalian homolog HJURP, may play
212 a role in the DDR pathway.
213
214 **The loss of Scm3 generates more Rad52 foci**

215 Having shown that the *scm3* mutant is sensitive to DNA damage, we hypothesized that the
216 mutant cells might be deficient in repairing intrinsic and extrinsic DNA damages. To examine
217 this, we wished to visualize the Rad52-GFP foci in these cells with or without MMS-induced
218 DNA damage. Since in budding yeast, the primary pathway to repair DNA damage is through
219 homologous recombination (HR) mediated by Rad52, deficiency in repair will cause
220 accumulation of DNA lesions and hence Rad52 (Dornfeld and Livingston, 1991; Lisby et al.,
221 2003, 2001). The mid-log grown *RAD52-GFP SCM3-AID* cells were split into auxin- and
222 DMSO-treated halves. Following 2 hrs of treatment, the cells were again split and were mock-
223 treated or treated with 0.02% MMS for 90 mins (Figure 2A). We visualized the formation of
224 Rad52-GFP foci in these cells (Figure 2B). Interestingly, we observed that 18% of the Scm3
225 depleted (+auxin) cells showed Rad52-GFP foci in contrast to only 5% in the wild type (Figure
226 2C, untreated). In accord with this, when these cells were challenged with MMS, a significant
227 increase of cells with Rad52-GFP foci was observed in the mutant (70%) compared to the wild
228 type (45%) (Figure 2C, 0.02% MMS). Moreover, while the mutant cells harbored an average
229 of ~ 3 foci, the wild type showed ~2 foci per cell (Figure 2D) in response to MMS treatment.
230 These results suggest that both intrinsically and extrinsically generated DNA lesions remain
231 unrepaired in the absence of Scm3.

232 To understand the dynamics of Rad52 foci formation in *scm3* cells, we used a strategy
233 as shown in Figure S4A. Briefly, the *bar1Δ RAD52-GFP SCM3-AID* cells were arrested in the
234 G1 phase of the cell cycle by adding alpha factor. 1 hour before release from the G1 phase,
235 cells were treated with auxin to deplete Scm3 or with DMSO control. Subsequently, the cells
236 were washed several times and released into alpha factor free media supplemented with or
237 without MMS but in the presence of nocodazole in order to have all the cells eventually
238 arrested at metaphase. Following release, the cells were harvested every 30 mins and the
239 percentage of cells containing Rad52-GFP foci were visualized (Figure S4B). Scm3 depleted
240 cells, but not the wild type, with or without MMS, showed a peak of Rad52-GFP accumulation
241 at around 60 mins from G1 release (Figure S4C, D). Notably, this time point possibly coincides
242 with the timing of DNA replication (judged by bud morphology) when DNA is most susceptible
243 to intrinsic and extrinsic damages. Taken together, Scm3-depleted cells exhibit more Rad52
244 foci, indicating a compromised DDR pathway in these cells.

245 If the DNA lesions remain unrepaired, the cells might undergo an apoptotic pathway
246 leading to cell death. To determine the percentage of cell death in the *scm3* mutant culture,
247 the cells harvested at 90 mins of MMS or mock treatment (after auxin treatment), as shown in
248 Figure 2A were stained with propidium iodide (PI), which does not permeate the live cells and
249 stains only the dead cells (Figure S4E, arrow). We observed that while ~15% of the Scm3
250 depleted (+auxin, -MMS) cells were PI positive, it was only ~4% for the wild type (DMSO, -
251 MMS) (Figure S4E, untreated). The PI positive cell population increased after MMS treatment
252 in both the cultures with significant difference between them (35% vs 27%) (Figure S4E, 0.02%
253 MMS). These results suggest that unrepaired intrinsic and extrinsic DNA lesions in the
254 absence of *scm3* lead to compromised cell viability.

255 **Scm3 associates with non-centromeric sites in response to DNA damage**

256

257 Having observed that Scm3 depleted cells are compromised in DNA damage repair and *scm3*
258 interacts genetically with *rad52Δ*, it is reasonable to argue that Scm3 goes to the DNA damage
259 sites to promote repair. To examine this, we first wanted to see if Scm3 alters its localization
260 pattern in response to MMS-mediated DNA damage. Since Scm3 is also expected to localize
261 at the kinetochores (Mizuguchi et al., 2007), we visualized Scm3 along with the kinetochore
262 marker, Ndc10, on chromatin spreads. The cells harboring *NDC10-6HA SCM3-13MYC* were
263 mock-treated or treated with 0.02% MMS for 90 mins. Ndc10 showed bright foci representing
264 the kinetochore cluster, whereas Scm3 was localized to multiple locations across chromatin,
265 including its colocalization with Ndc10 (Figure 3A, arrow). Similar localization of Scm3 has
266 been observed earlier in live cells where Scm3-GFP showed a wider nuclear localization,
267 which might argue for its genome-wide functions (Luconi et al., 2011; Wisniewski et al., 2014).
268 We also observed a significant enrichment of Scm3 at the rDNA loops irrespective of the
269 extrinsic DNA damage (Figure 3A, arrowhead). The enrichment of Scm3 at the rDNA loops is
270 perhaps to maintain the highly repetitive organization of rDNA. HJURP has also been shown
271 to localize rDNA arrays in mammalian systems (Kato et al., 2007). Additionally, upon
272 quantifying the total intensity of Scm3-13Myc and Ndc10-6HA and normalizing that with the
273 background intensity, we observed a statistically significant increase in the Scm3-13Myc, but
274 not Ndc10-6HA intensity in response to MMS treatment (Figure 3B). No change in the intensity
275 of Ndc10-6HA post-MMS treatment justifies the absence of increased sensitivity of Ndc10
276 depleted cells in response to MMS (Figure S3A).
277 Having observed an increased chromatin localization of Scm3 in response to MMS on
278 chromatin spreads, we wished to verify this by determining genome wide association of Scm3
279 using ChIP-Seq. To negate any effect on Scm3's binding due to cell cycle progression we first
280 arrested the cells harboring *SCM3-13MYC* at metaphase by nocodazole. The arrested cells

281 were further mock treated or treated with 0.05% MMS for an additional 90 mins before they
282 were harvested for ChIP. The Scm3 ChIP-seq signal was normalized with the input signal,
283 and genome-wide plots were generated to see Scm3 binding along the entire chromosomes.
284 We also performed ChIP-seq from a no-tag control strain that provided the background signal
285 due to the antibody or the beads treatment. We could observe an enrichment of Scm3 in both
286 MMS treated and untreated cells at the centromeres, while no enrichment in the no-tag sample
287 was observed (Figures 3C, 3D, S5). In the untreated sample, the peaks called by MACS2 after
288 input normalization showed enrichment of Scm3 at a few other genomic locations as well
289 besides the centromeres (Figures 3C, 3D, S5, green arrows), which was also observed in our
290 chromatin spread data (Figures 3A, 3B). Interestingly, in MMS treated cells, following same
291 methodology, we could observe a greater number of peaks of Scm3 binding to the non-
292 centromeric locations (Figures 3C, 3D, S5, black arrows). While in the untreated sample,
293 Scm3 localized to 1-2 non-centromeric locations, the same increased drastically in the treated
294 sample. Such non-centromeric chromatin enrichment of Scm3 was observed for several
295 chromosomes (S5, black arrows) and corresponds to the increased chromatin localization of
296 Scm3 in response to MMS, as visualized on chromatin spreads (Figure 3B). Further, we could
297 observe the localization of Scm3 at the 9.1 kb rDNA region on ChrXII, validating our chromatin
298 spread data (Figure 3E).
299
300 **Scm3 partially co-localizes with Rad52, perhaps at the DNA damage sites**
301
302 Given the increased chromatin association of Scm3 in response to DNA damage we wished
303 to investigate if this occurs due to its binding to the DNA damage sites. For this, we examined
304 the colocalization of Scm3 with Rad52 upon DNA damage, as the latter is known to be targeted
305 to the damage sites (Lisby et al., 2003; Miyazaki et al., 2004). To visualize both Rad52 and
306 Scm3 simultaneously on chromatin spreads, cells harboring *RAD52-6HA* and *SCM3-13MYC*
307 were mock-treated or treated with 0.02% MMS for 90 mins. We did not observe any significant
308 co-localization between Scm3-13Myc and Rad52-6HA in untreated cells as judged by low
309 Pearson's Correlation Coefficient value (PCC < 0.4) (Figure 4A-B). However, in the cells
310 treated with MMS, we could observe a significant increase in the PCC value (PCC > 0.5)
311 (Figure 4B). This indicates a partial co-localization between Scm3 and Rad52 in the presence
312 of the DNA damage and implicates that Scm3 may localize to the damage sites in response
313 to DNA damage.
314 Next, we wished to examine the behavior of Scm3 with respect to another DNA
315 damage marker. In mammals, the DSB sites are marked by γ-H2Ax due to phosphorylation of
316 the H2A variant, H2Ax, by ATM/ATR kinases (Burma et al., 2001; Lee et al., 2014) In yeast
317 that lacks H2Ax, the DSBs are marked by γ-H2A due to phosphorylation of histone H2A by

318 Mec1 and Tel1 kinases (Lee et al., 2014). To be noted, γ-H2A is also found at the
319 heterochromatin region and co-localizes with yeast heterochromatin protein Sir3 (Javaheri et
320 al., 2006; Kirkland et al., 2015; Kitada et al., 2011). We performed a chromatin spread assay
321 using antibodies specific to γ-H2A and observed a drastic increase in the intensity of γ-H2A
322 when the cells were subjected to DNA damage, which is expected (Figure S6 A, B). To verify
323 that the phenomenon is DNA damage associated, we observed a significant increase in the
324 colocalization between Rad52 and γ-H2A in response to DNA damage (Figure S6 C-D). To
325 further correlate the localization of Scm3 with DNA damage, we then visualized both Scm3-
326 13Myc and γ-H2A simultaneously on chromatin spreads from *SCM3-13MYC* cells mock-
327 treated or treated with 0.02% MMS for 90 mins before they were harvested for the assay. We
328 did not observe any significant co-localization between Scm3-13Myc and γ-H2A in untreated
329 cells as judged by low Pearson's Correlation Coefficient value (PCC < 0.3) but found a
330 significant increase in the value (PCC > 0.6) in MMS treated cells (Figure 4C-D). Taken
331 together, we conclude that the association of Scm3 with chromatin and its co-localization with
332 DDR proteins increases with DNA damage.
333
334 **Scm3 is recruited to a site-specific DSB**
335 The overall increased association of Scm3 with the chromatin and its colocalization with
336 Rad52 and γ-H2A in response to MMS-mediated DNA damage prompted us to examine if
337 Scm3 is recruited specifically to DNA damage sites. For this, we utilized the chromatin
338 immunoprecipitation (ChIP) assay to visualize the dynamics of Scm3 recruitment at an
339 induced DSB site. We used a yeast strain (NA14) harboring an HO cut site integrated at the
340 mutant *ura3* locus, which is cleavable by HO endonuclease upon galactose induction (Agmon
341 et al., 2009; Fangaria et al., 2022). The strain also contains a distant *URA3* locus, which is
342 utilized to repair the cut *ura3* locus post-DSB induction. The cleavage by HO endonuclease
343 was first verified by PCR-based analysis using primers complementary to the DNA sequence
344 flanking the HO cut site (Figure 5A). The DNA damage was maximal at 2 hrs of galactose
345 induction, and the damage was majorly repaired by 4 hrs of galactose induction (Figure S7 A,
346 B).
347 We monitored the recruitment of Scm3 near DSB and at sites distal to that up to -3 kb
348 (Figure 5A) by performing ChIP of Scm3-6HA from the samples collected at every hr up to 4
349 hrs following galactose induction. As a positive control for Scm3 ChIP, we found significant
350 enrichment of Scm3 at the centromere (*CEN3)* (Figure S7C). We observed a significant
351 increase in the Scm3 binding near DSB at 2 hrs of galactose induction and a decrease in the
352 enrichment at 4 hrs, possibly due to the gradual repair of the damage (Figure 5B, C). We also
353 observed an increase in the enrichment of Scm3 up to -3 kb sites distal to the cut site, which

354 decreased gradually with damage repair (Figure 5C) and no significant enrichment at the
355 *TUB2* locus, used as negative control (Figure 5C) or in the no antibody control (Figure 5D).
356 This suggests that Scm3 is maximally recruited to the cleavage sites at the time of DNA
357 damage and gradually dissociates as and when the DNA is repaired. To verify that HO-
358 induced DSB is able to recruit the DNA repair proteins, we also investigated the enrichment
359 of such a protein, Rad51, that is known to bind the DSB sites (Fangaria et al., 2022) and found
360 it is maximally enriched at these sites during 2-3 hrs of post-galactose induction (Figure S7D).
361 We conclude that upon DNA damage Scm3 associates with the damage sites and may act in
362 *cis* to facilitate damage repair.
363
364 **Activation of the DDR checkpoint is perturbed in the *scm3* mutant.**
365
366 Having shown the recruitment of Scm3 at the DNA damage sites, we wished to address the
367 role of Scm3 at these sites in case of DNA damage. Since we found that Scm3 depleted cells
368 are compromised in repairing DNA damage, it is possible that being at the damage sites Scm3
369 activates the DDR checkpoint, which is required for the damage repair. In the DDR pathway,
370 Rad53 is an effector kinase that becomes phosphorylated in a Mec1 sensor kinase-dependent
371 manner in response to DNA damage (Ciccia and Elledge, 2010; Melo and Toczyski, 2002;
372 Zhou and Elledge, 2000). Phosphorylation of Rad53 is essential to halt the cell cycle and
373 provide cells time to repair the damaged DNA. To examine whether Scm3 depleted cells have
374 defects in the activation of DDR checkpoint and in halting the cell cycle, we measured Rad53
375 phosphorylation status in the wild type and the Scm3 depleted cells after treating them with
376 0.02% MMS for 90 mins (Figure 6A). Anti-Rad53 antibodies that recognize both
377 phosphorylated and unphosphorylated forms of Rad53 were used. We observed lesser
378 phosphorylation of Rad53 in the *scm3* than in the wild-type cells treated with MMS, but no
379 difference was found in the untreated cells (Figure 6B).
380 Since Scm3-depleted cells, unlike the wild type, arrest at the G2/M stage due to
381 activation of spindle assembly checkpoint (SAC) (Camahort et al., 2007; Stoler et al., 2007),
382 the observed difference in Rad53 phosphorylation could be due to the difference in cell cycle
383 stages. To circumvent this issue, we grew *CDC20-AID* and *SCM3-AID* cells for 3 hrs before
384 treating them with 0.75 mM auxin for 2 hrs to arrest them first at G2/M by depleting Cdc20 and
385 Scm3, respectively (Figure 6C). The cells were then treated with 0.02% MMS and harvested
386 at indicated time points for total protein extraction. The *CDC20-AID* and *SCM3-AID* cultures
387 showed around ~80% metaphase arrest cells, in 2 hrs of auxin treatment (0 mins in Figure
388 S8A). Notably, while the Cdc20-depleted cells maintained the arrest even with a longer
389 incubation in auxin, the Scm3-depleted cells tend to bypass the arrest after a certain time and
390 showed accumulation of multibudded cells with fragmented DAPI, an arrest-release

391 phenotype (Figure S8B, Figure 6E) Consistent with our previous results (Figure 6C), we
392 observed that in Scm3 depleted cells, Rad53 is less phosphorylated than in Cdc20-depleted
393 cells (Figure 6D), in particular, while comparing the bands at 120 mins when the percentage
394 of metaphase cells was found similar in two cultures (Figure S8B). These results indicate that
395 in the absence of Scm3, when there is DNA damage, the activation of the DDR checkpoint is
396 improper, and consequently, the phosphorylation of Rad53 is compromised.

397 If the loss of Scm3 fails to activate the damage checkpoint properly, then it is expected
398 that the cell cycle arrest phenotype in response to DNA damage would also be defective and
399 would produce multibudded cells. We wished to examine this possibility. However, Scm3-
400 depleted cells arrest by spindle assembly checkpoint (SAC) at G2/M due to improper
401 kinetochore-microtubule attachment because of failure in Cse4 deposition (Camahort et al.,
402 2007; Stoler et al., 2007). To exclude the effect of SAC-mediated arrest, we deleted the SAC
403 component *MAD2* in *SCM3-AID* cells. These cells were first depleted of Scm3 by treatment
404 with auxin and then, along with *mad2Δ* control cells, were challenged with or without MMS for
405 90 mins before they were analyzed for percentage of multi budded cells (Figure 6E). While
406 the *mad2Δ* cells in the presence of MMS showed nominal multi budded cells (<5%), the same
407 cells upon depletion of Scm3 showed a steep rise in the phenotype (>40%), suggesting that
408 Scm3 depleted cells fail to activate DNA damage checkpoint and to arrest the cell cycle in the
409 presence of DNA damage.

410 Since Scm3 depleted cells showed reduced Rad53 phosphorylation, we wished to
411 examine if the lack of Scm3 perturbs Mec1 kinase function that phosphorylates Rad53. Mec1
412 phosphorylates histone H2A at S129 position upon DNA damage (Lee et al., 2014). However,
413 we failed to observe any significant difference in the phosphorylation status of H2AS129
414 between Scm3, or Cdc20 depleted cells (Figure S8C), indicating that the Mec1 function is not
415 perturbed in the absence of Scm3.

416

417 **Phosphorylation of Scm3 in response to DNA damage**

418 The function of Scm3 in DDR could be mediated by a damage-induced post-translational
419 modification of this protein. To examine if Scm3 becomes modified upon DNA damage, we
420 treated *SCM3-6HA* cells with increasing concentrations of MMS or with 0.02% MMS with
421 increasing duration. We observed slower migrating bands of Scm3 (Scm3*) that became
422 brighter with increasing concentrations of MMS and present very faintly even in the untreated
423 cells (Figure 7A, left panel). We observed an increase in the normalized intensity of Scm3*
424 and Scm3*/Scm3 ratio with increasing MMS concentration (Figure 7A, middle, and right
425 panels). A similar observation was also made when the cells were treated with 0.02% MMS
426 for increasing time (Figure S9A). Since we could detect Scm3* bands in the untreated cells as

427 well, its enrichment in response to MMS could be due to a cell cycle arrest caused by MMS.
428 To understand the dynamics of the appearance of Scm3* bands over different cell cycle stages
429 and in response to MMS, we released the *bar1*Δ *SCM3-6HA* cells from alpha-factor mediated
430 G1 arrest into the medium in the absence or presence of MMS, as shown in Figure 7B. We
431 harvested the cells at indicated time points and evaluated the cell cycle synchrony using bud
432 morphology and DAPI staining (Figure 7C, Figure S9 B, C), which depicts that the majority of
433 the cells at 0, 30, 60, 90, and at 120 mins are in G1, S, metaphase, metaphase/anaphase and
434 anaphase, respectively. We could faintly observe the Scm3* bands after release from the G1
435 phase in MMS-free (untreated) media, and the band intensity did not change over the time
436 period. However, when the cells were released in the presence of MMS, we observed an
437 increase in the intensity of the Scm3* bands over time (Figure 7D). These results suggest that
438 the accumulation of Scm3* in the MMS treated cells is due to DNA damage rather than an
439 effect of the pace of the cell cycle. It is possible that Scm3* bands are phosphorylated forms
440 of Scm3 since the protein has several serine/threonine residues. To test this, we challenged
441 the Scm3-6HA cells with MMS, as in Figure 7A, and resolved the proteins on SDS-PAGE with
442 or without Phos-Tag reagent. The presence of Phos-Tag in the gel enables slow mobility of
443 the phosphorylated proteins and thus further differentiates them from their unphosphorylated
444 forms. Figures S9D and E show the migration of the proteins isolated from *SCM3-6HA* cells
445 challenged with different concentrations of MMS in the absence or presence of Phos-Tag
446 reagent, respectively. The mobility of the Scm3* bands was further reduced with respect to
447 the Scm3 band in Phos-Tag gel compared to the normal gel, suggesting that the modification
448 is likely due to phosphorylation. Notably, in several high throughput studies, Scm3 has been
449 shown to be phosphorylated at S39, S64, and S165 residues (Lanz et al., 2021; MacGilvray
450 et al., 2020; Zhou et al., 2021). The S64 phosphorylation of Scm3 was found to be enriched
451 in cells after MMS treatment for 2 hrs as compared to G1 arrested cells, although the authors
452 could find S64 phosphorylation in only 2 out of 4 replicates used in their study (Lanz et al
453 2021). However, in the absence of further validation in those studies, our observation of a
454 gradual increase in the Scm3* band intensity with increasing dose of MMS convincingly
455 demonstrate DNA damage dependent phosphorylation of Scm3.
456 Since, Mec1 kinase majorly contributes to the activation of DDR through protein
457 phosphorylation, we tested if Scm3 undergoes a Mec1-dependent phosphorylation in
458 response to MMS. We constructed the *sml1*Δ *mec1*Δ *SCM3-6HA* strain as *mec1*Δ cells are
459 viable in the absence of Sml1 (Zhao et al., 2001, 1998) and challenged this and other control
460 strains with MMS. Briefly, wild type, *SCM3-6HA*, *sml1*Δ*SCM3-6HA*, and *sml1*Δ *mec1*Δ *SCM3-*
461 *6HA* cells were grown till mid-log and spotted on the plates containing MMS (Figure S9F). As
462 expected, the *sml1*Δ *mec1*Δ *SCM3-6HA* cells showed extreme sensitivity to MMS. However,
463 we could not observe any loss of Scm3 phosphorylation in the *sml1*Δ *mec1*Δ background in

464 the presence of MMS, suggesting that Scm3 phosphorylation in response to DNA damage is
465 not dependent on Mec1 kinase activity (Figure S9G).
466
467 **Discussion**
468 The bonafide function of the Cse4 chaperone, Scm3, is to deposit Cse4 at the centromeres
469 during the S phase in budding yeast to facilitate kinetochore formation. The observation that
470 Scm3 persists not only at the centromeres throughout the cell cycle but also associates with
471 the gross chromatin argues for additional kinetochore-independent functions of Scm3 in
472 maintaining genome stability. While in metazoan, Scm3 homolog HJURP was initially
473 identified as a protein involved in DNA damage response (DDR), how HJURP regulates the
474 DDR pathway besides its role in CENP-A deposition is not well understood. The DDR role of
475 Scm3 has never been reported in budding yeast. Whether Scm3 also contributes to DDR
476 pathway in budding yeast is important to address since this organism is distinct from
477 metazoans in terms of harboring small 125 bp point centromeres contrasting megabase pair
478 large regional centromeres in metazoans and having lesser epigenetic control on biological
479 functions, including DNA damage repair. Here, for the first time, we report that Scm3, perhaps
480 upon phosphorylation, promotes DNA damage repair by contributing to the activation of the
481 DNA damage checkpoint, and in the process, it associates with the DDR proteins at the DNA
482 damage sites (Figure 8). Our findings have a significant impact on advancing knowledge of
483 how CENP-A chaperones can be involved in the DDR pathway.
484
485 **Lack of Scm3 increases DNA damage sensitivity**
486 It is technically challenging to perform a growth-based sensitivity assay using cells depleted
487 for an essential gene. To circumvent this issue with Scm3, which is essential for cell survival,
488 we used partial depletion of Scm3 to assess the sensitivity of the partially depleted cells to the
489 genotoxic agents, including MMS, HU, and CPT and observed that such cells were sensitive
490 to those agents, (Figure 1, Figure S2A). However, since the primary function of Scm3 is to
491 promote kinetochore formation by depositing Cse4 at the centromeres, it is important to
492 address if the observed sensitivity is due to perturbation in kinetochores. Therefore, we
493 similarly partially depleted two essential kinetochore proteins, Ndc10 and Mif2, and deleted
494 one non-essential kinetochore protein, Ctf19, in separate cells but failed to detect any
495 increased sensitivity to DNA damage stress (Figure S3). These results indicate that the drug
496 sensitivity phenotype of Scm3 depleted cells is not due to weakly formed kinetochores. The
497 arguments favoring the possible centromere-independent DDR functions of Scm3 can be
498 gleaned as follows. From comparing the domain organization of Scm3 with HJURP (Figure
499 S1A), we noticed that besides the CENP-A/Cse4 binding domain, both HJURP and Scm3
500 have a common DNA binding domain, which is dispensable for CENP-A/Cse4 binding and

501 also for Ndc10 binding in budding yeast. Both in vitro and in vivo evidence are there
502 demonstrating binding of the DNA binding domain to the DNA (Kato et al., 2007; Mizuguchi et
503 al., 2007), suggesting this domain can indeed recruit Scm3 also at the non-centromeric DNA
504 damage sites. In support of this, Scm3 has recently been shown to be phosphorylated in an
505 MMS-dependent manner at S64 (Lanz et al., 2021), which, interestingly, lies within the DNA
506 binding domain. Among other non-essential regions of Scm3, neither the NLS region nor the
507 C-terminal region is involved in DDR (Figure S1B). On the other hand, the D/E-rich region,
508 which is important for Scm3 stability (Stoler et al., 2007), forms a disordered domain as per
509 alpha-fold prediction and hence is believed to be capable of interacting with multiple proteins
510 or can act as a scaffold for engaging several protein-protein interactions which is required in
511 DDR.
512 MMS halts replication forks due to the formation of DNA adducts, which eventually
513 generate recombinogenic lesions (Conde and San-Segundo, 2008). In yeast, these lesions
514 are repaired primarily through homologous recombination (HR), facilitated by the Rad52
515 epistasis group of proteins (Pizzul et al., 2022; Sirbu and Cortez, 2013). Rad52, the central
516 component of the HR pathway, deposits Rad51 onto the broken DNA strand, which then
517 searches for the homologous template and undergoes strand exchange to repair the broken
518 DNA (Haber, 2018). In the presence of any DNA damage, Rad52 relocalizes to form bright
519 foci, which mark the repair centres. Strikingly, we observed that the Rad52 foci are increased
520 drastically in the absence of Scm3, even without any external DNA damage (Figure 2C, Left).
521 The maximal accumulation of Rad52-GFP foci was noticed during the 60 mins post-G1
522 release, which coincides with the timing of DNA replication (Figure S4C), indicating that Scm3
523 might be required to avoid generating DNA lesions during replication, which itself is genotoxic.
524 In support of this, previously, it was observed that a significant cell population arrests during
525 the S phase in the absence of Scm3 (Camahort et al., 2007). As expected, the accumulation
526 of Rad52-GFP foci was significantly higher in the *scm3* mutant as compared to the wild-type
527 cells when they were treated with MMS, suggesting that cells become more vulnerable to DNA
528 damage in the absence of Scm3 (Figure 2C, Right).
529
530 **Association of Scm3 with non-centromeric loci**
531
532 In addition to the localization of Scm3 at the kinetochores, we also found it at other loci,
533 including at the ribosomal DNA (rDNA) loops (Figure 3A, arrowhead). In budding yeast,
534 chromosome XII, harbors rDNA with around 150 repetitive loci (Dammann et al., 1993; Smith,
535 2022). Recombination among these repeats excise rDNA circles, and therefore, efficient DNA
536 damage repair through HR at these loci is crucial for preserving genomic stability. Notably,
537 HJURP has been identified in mammals to bind to the rDNA region and maintain its stability

538 (Kato et al., 2007). The degradation of HJURP using siRNA resulted in increased rDNA
539 recombination events and chromosome instability (Kato et al., 2007). The presence of Scm3
540 at the rDNA loops suggests that Scm3, like HJURP, is also important in regulating the
541 recombination and repair processes at those loci (Figure 3D).

542 Both Rad51 and Rad52 have been shown to mark the site of recombination and repair
543 (Lee et al., 2003; Lisby et al., 2001; Miyazaki et al., 2004). In our assay, we observed a
544 statistically significant co-localization of Scm3 with Rad52 in response to DNA damage (Figure
545 4A). Since during DSB repair, multiple lesions are recruited to a few repair centers, which are
546 marked by Rad51 and Rad52, the colocalization of these proteins with Scm3 implicates the
547 recruitment of Scm3 at the repair centers. Moreover, an overall increase in the chromatin
548 association of Scm3 in response to MMS also suggests that Scm3 is recruited to several repair
549 centers (Figure 3B, C, E, S5). However, as expected, no such increase in the chromatin
550 association was observed for an inner kinetochore protein, Ndc10. It is possible that Scm3
551 might physically interact with Rad51/Rad52 through the HR or DNA binding domain or the D/E
552 rich region present in the protein (Figure S1A). However, we failed to observe any interaction
553 of Scm3 with Rad52 using co-IP assay.

554 DNA damage sites are epigenetically marked by phosphorylation of H2AS129 (γ-H2A)
555 through the ATM/ATR kinase pathway (Burma et al., 2001; Lee et al., 2014). However, in
556 budding yeast, γ-H2A is also recruited at the heterochromatin regions (Kitada et al., 2011). In
557 unperturbed cells, we could visualize γ-H2A foci (Figure 4C), possibly due to its presence at
558 the stalled replication forks, fragile sites, telomeric regions, or at the heterochromatin regions
559 (Kirkland et al., 2015; Kitada et al., 2011; Rg Bewersdorf et al., 2006). The increase in intensity
560 of γ-H2A upon MMS treatment (Figure S6A, B) indicates the presence of γ-H2A at multiple
561 DNA damage sites. The significantly high co-localization of Scm3 (PCC > 0.6) with γ-H2A in
562 the MMS treated cells, therefore, indicates that Scm3 is indeed recruited to the DNA damage
563 sites (Figure 4D). This was further verified by using an ectopic DSB system, where we showed
564 the recruitment of Scm3 to the induced DSB sites (Figure 5B). Notably, Scm3's presence was
565 found not only limited to the regions very close to the cut site but also up to 3 kb distal from
566 there. This may be the reason for observing a high co-localization of Scm3 with γ-H2A in
567 response to MMS, as the latter also spreads distal to the cut site (Lee et al., 2014). Although
568 Scm3 binding at the cut site peaked at 2 hrs following HO induction, the time of maximal DNA
569 cleavage, it persisted for at least 3-4 hrs post induction even when ~60% of the cut DNA was
570 repaired. This suggests that Scm3 is recruited to the sites of DNA damage and persists there
571 during the repair process.

572

573 **Scm3 regulates DNA damage checkpoint**

574 We wanted to address the mechanism by which Scm3 might be involved in DDR. The DNA
575 damage checkpoint arrests the cell cycle in response to DNA damage, allowing cells to repair
576 the damage and maintain cell viability. The serine/threonine kinases Mec1/Tel1 in yeast are
577 the sensor kinases that are activated and recruited to the sites of DNA damage. These kinases
578 relay the signal downstream by phosphorylating and activating the effector kinases, including
579 Chk1 and Rad53 (Pizzul et al., 2022; Zhou and Elledge, 2000). The activation of the effector
580 kinases is critical for activating the further downstream substrates that eventually halts the cell
581 cycle. We observed a defect in the Rad53 phosphorylation in response to MMS-mediated DNA
582 damage in the absence of Scm3 (Figure 6B). Failure to activate Rad53 in the presence of
583 damage leads to improper G2/M cell cycle arrest, which can produce the multi-bud phenotype.
584 In the Scm3 depleted cells deleted for Mad2 to remove the ability of SAC mediated arrest (due
585 to kinetochore perturbation), we observed a significant population of multibudded cells (Figure
586 6E) when they were challenged with MMS. Only *mad2*Δ cells challenged with MMS did not
587 show such multi-bud phenotype, suggesting that Scm3 is important to arrest the cells in
588 response to DNA damage. Next, we wished to know why the Scm3 depleted cells are
589 compromised to phosphorylate Rad53. It is known that Rad9 acts as an adaptor upon
590 phosphorylation by upstream Mec1 kinase to phosphorylate Rad53 (Gilbert et al., 2001;
591 Pellicioli and Foiani, 2005). To test if lack of Scm3 attenuates Mec1 activity, we tested the
592 level of γ-H2A in the Scm3 depleted cells as Mec1 activity is also responsible to generate γ-
593 H2A (Burma et al., 2001; Lowndes and Toh, 2005). However, the level of γ-H2A was not
594 perturbed in the *scm3* mutant, suggesting that Mec1 activity is intact (Figure S8C). Therefore,
595 currently, we are uncertain about the cause of improper Rad53 phosphorylation; a defect in
596 its auto-activation property or in the action of some other mediator kinases, e.g., Tel1, may be
597 responsible, which can be tested. Nevertheless, given the increased phosphorylation of Scm3
598 in response to DNA damage, it is possible that the p-Scm3 is required to activate Rad53
599 (Figure 7A). Although we found that Scm3 phosphorylation is Mec1 independent (Figure S9G),
600 it is possible that other kinases are involved. While the involvement of CDKs in the DNA
601 damage checkpoint is not well understood, it is known that CDKs contribute to the
602 phosphorylation of both Rad52 and Rad51 to promote repair (Lim et al., 2020). Given that the
603 centromeric association of Scm3 varies with the cell cycle stage (Mishra et al., 2011), probably
604 due to oscillating levels of CDK activity, the DNA damage-dependent phosphorylation of Scm3
605 might also be regulated by CDKs. However, this does not rule out the involvement of other
606 kinases including Rad53 and Tel1, which are closely associated with the DNA damage
607 checkpoint pathway. Further investigation is required to precisely determine the kinase
608 involved in the Scm3 phosphorylation.

In summary, we report here that, like HJURP, Scm3 in budding yeast also possesses functions in DDR, indicating that the centromere independent functions of the CenH3 chaperone are evolutionarily conserved. Although the chromatin landscape of budding yeast is far more 'open' with lesser involvement of epigenetic determinants than in metazoans, the inherent similarity in the DNA damage repair pathway may necessitate the utilization of these chaperones in a similar fashion in both cell types. Not much has been studied about how HJURP is involved in the DDR pathway, and as we reveal that Scm3 is involved in the proper activation of the DNA damage checkpoint in the presence of DNA lesions (Figure 8), the same can be tested for HJURP in metazoans as abrogation of such surveillance function in humans can lead to aneuploidy and disease states. Our findings on Scm3 will pave the way for future work using yeast as a model to decipher more genome wide functions of the CenH3 chaperone, which is crucial given its genome wide localization and evidence of its modulation in several patients.

Acknowledgement:

We acknowledge Prof. Martin Kupeic from Tel Aviv University, Israel, for providing us with the NA14 strain. SKG is supported by a grant (BT/PR43050/BRB/10/1992/2021) from the Department of Biotechnology (DBT), Govt of India. PA is supported by CSIR fellowship (09/087(0972)/2019- EMR-I).

Author contributions: PA performed experiments. PA and SKG designed experiments, analyzed and interpreted the data. PA and SKG wrote the manuscript.

Materials and Methods:

Yeast strains

All *Saccharomyces cerevisiae* strains used in this study are derived from W303 genetic background and are mentioned in Table S1. Standard growth conditions were used to grow and harvest yeast for all the experiments. C-terminal tagging (AID, HA, Myc, GFP) or gene deletions were performed using PCR-based integration at endogenous locations as described before (Janke et al., 2004; Longtine et al., 1998; Wach, 1996). Standard lithium acetate-based yeast transformation methods were employed for all genetic manipulations (Gietz and Woods, 2002).

Media, reagents and growth conditions

Yeast strains were grown using standard growth conditions (Sherman, 2002). For plates containing MMS, HU and CPT (Sigma Chemicals, Switzerland), the drugs were top-plated on

644 YPD plates at appropriate concentrations. To arrest the cells at the G1 or metaphase stage of
645 the cell cycle, alpha factor (Sigma Chemicals, Switzerland) or nocodazole (Sigma Chemicals,
646 Switzerland) was added to the cells at indicated concentrations. For HO endonuclease
647 induction, strains were grown on a rich medium containing 3% glycerol prior to the addition of
648 3% galactose. For western blotting, immunoprecipitation, or immunofluorescence studies the
649 primary antibodies used were rat anti-HA (3F10, Roche), mouse anti-HA (12CA5, Roche),
650 mouse anti-Myc (9E10, Roche), rat anti-tubulin (MCA78G, Serotec), rabbit anti-Rad53
651 (ab104232, Abcam), rabbit anti-Rad51 (PA5-34905, Invitrogen) and rabbit anti-Histone H2A
652 (phospho-S129) (ab15083, Abcam). The secondary antibodies used were Rhodamine
653 (TRITC)-conjugated goat anti-Rat (Jackson), Alexa Fluor 488 conjugated goat anti-Mouse IgG
654 (Jackson), Rhodamine (TRITC)-conjugated goat anti-Rabbit, HRP-conjugated goat anti-
655 mouse IgG (Jackson), HRP-conjugated goat anti-rat (Jackson), HRP- conjugated goat anti-
656 rabbit (Jackson) at appropriate dilutions.
657
658 **Cell spotting and viability assay**
659
660 The cells were grown in standard media conditions till the mid-log phase. The cultures were
661 then 10-fold serially diluted and spotted on the plates containing auxin (dissolved in DMSO)
662 or other DNA-damaging agents. All the reagents were top-plated onto YPD or specific dropout
663 plates. After spotting, the plates were incubated at 30°C for 2-3 days before they were
664 photographed, depending on the growth rate.
665 For treatment of the cells in liquid culture, mid-log grown cells were treated with auxin
666 (dissolved in DMSO) or MMS for the indicated time points before they were harvested and
667 spotted on YPD plates or plates containing DNA damaging agents. To measure cell viability,
668 an equal number of cells were plated on drug free or drug containing YPD plates. The cells
669 were grown at 30°C for 2 days, and the number of viable colonies was counted. The colonies
670 formed on the drug free plate were taken as 100% viability, and accordingly the viability
671 percentage was calculated and plotted for drug containing plates.
672
673 **G1 arrest and release**
674
675 Cells were arrested in the G1 phase by adding 0.5 µg/mL α-factor to early log phase cells in
676 liquid culture (Amon, 2002). The cells were incubated for 2-3 hours or until at least more than
677 90% of cells showed shmoo morphology. For the release of the cells from α-factor arrest, the
678 cells were harvested and washed twice with pre-warmed water at 30°C which was followed
679 by washing twice with pre-warmed α-factor free media at 30°C with at least 10 times the

volume of the initial culture. The cells were then released in α-factor free media, and samples were collected at different time points.

Fluorescence imaging

For live cell imaging, the samples were harvested at indicated time points and washed twice in 0.1 M phosphate buffer before imaging. The cells were processed for DAPI staining, as mentioned elsewhere (Mittal et al., 2020; Shah et al., 2023). Typically, the cells were fixed with 4% formaldehyde at RT for 5 mins. The fixed cells were washed twice with 0.1M phosphate buffer (pH 7.5), vortexed in freshly prepared 50% ethanol for 30 seconds, and rewashed with 0.1M phosphate buffer. Before imaging, the cells were resuspended in freshly prepared DAPI (1 µg/ml, Invitrogen) solution for 20 mins. The images were acquired through the Zeiss Axio Observer Z1 fluorescence microscope (63× or 100×) in z-stack mode (0.2-0.5 µm spacing).

Chromatin spread

Chromatin spread was performed, as mentioned previously (Ma et al., 2023; Mehta et al., 2014; Shah et al., 2023). Briefly, mid-log ($O.D._{600}$ = ~1.0) grown cells were harvested and washed once with spheroplasting buffer (1.2 M sorbitol in 0.1 M phosphate buffer). The cells were resuspended in 0.5 ml of the same buffer supplemented with 5 µl of β-mercaptoethanol and 12.5 µl of zymolyase 20T (10 mg/ml, MP Biomedicals, USA) and incubated at 30ºC for 1 h. Once 80-90% of the cells were spheroplasted (by observing under the microscope), the spheroplasting was stopped by adding 1 ml of ice-cold stop solution (0.1 M MES- pH 6.4, 1 mM EDTA, 0.5 mM $MgCl_2$, 1 M Sorbitol). The spheroplasts were centrifuged at 2000 rpm for 2 mins and resuspended in 120 µl of ice-cold stop solution. About 60 µl of spheroplasts were mounted on an acid-washed clean glass slide. The cells were treated with freshly made paraformaldehyde solution (4% paraformaldehyde, 3.4% sucrose), followed by 1% Lipsol (LIP Equipment and services) solution for cell lysis. The lysed cells were homogenously spread over the slide and air-dried at RT. After overnight drying, the slides were treated with 0.4% Kodak Photoflow-200 to avoid photobleaching, followed by 5% skim milk as a blocking solution, which was covered with coverslips. The coverslips were removed, and the slides were incubated with primary and secondary antibodies (1:200) for 60 mins with three times PBS washing between antibody treatments. The slides were then incubated with 100 µl of DAPI (1 µg/ml, Invitrogen) for 30 mins. After PBS wash for 5 mins, 100 µl of mounting solution (90% glycerol supplemented with 1 mg/ml p-phenylenediamine) was added over the slides. A clean coverslip was placed over a slide and was sealed with transparent nail paint.

718 **Microscopic image analysis**

719

720 The images acquired through the Zeiss Axio (Observer Z1) fluorescence microscope were
721 processed using Zeiss Zen 3.1 software. The z-stacks with the best signal for a particular
722 channel were extracted and merged separately. For intensity calculation, a Region Of Interest
723 (ROI) was drawn around the signal of interest, and the integrated density was determined to
724 get the 'signal intensity' for both channels. An ROI of the same size was put elsewhere in the
725 background, and integrated density was determined to get the 'background intensity.' Each
726 signal intensity value was normalized with the background intensity values to get the
727 'normalized signal intensity' which was used to plot the graphs (Shah et al., 2023).
728 For Pearson's correlation coefficient (PCC) values to determine the extent of co-
729 localization, the merged z-stacks were extracted, and the 'Coloc' tool from the 'Imaris 8.0.2'
730 software was used. The 'automatic thresholding option' in the 'Coloc' tool was used to
731 calculate the threshold for each fluorescence emission channel. The PCC values were
732 recorded separately for each individual spread. The colocalization was described as no (PCC
733 <0.1), partial (PCC = 0.3-0.5) and complete (PCC>0.5) (Ma et al., 2023; Prajapati et al., 2018;
734 Zinchuk and Grossenbacher-Zinchuk, 2014).

735

736 **Induction of a site-specific DSB**

737

738 NA14 (Fangaria et al., 2022) cells were grown till 0.3 OD in the presence of 3% glycerol. 5 OD
739 of the cells were harvested (0 h), and the remaining cells were treated with 3% galactose for
740 4 hrs. 5 OD cells were harvested every hour till 4 hrs. The cells were lysed using glass beads
741 in lysis buffer (2% Triton X-100, 1% SDS, 100 mM NaCl, 10 mM Tris pH 8, and 1 mM EDTA
742 pH 8.0), and total DNA was isolated as described before (Hoffman, 1997) and was solvent
743 extracted using PCI. The genomic DNA was precipitated and finally resuspended in 30 µl 1X
744 TE. The concentration of DNA was measured using a nano spectrophotometer. About 30 ng
745 of DNA was used for PCR to detect the DNA break using primers OSB289 and kanB1
746 (Fangaria et al., 2022). Primers against *TUB2* ORF were taken as a control.

747

748 **ChIP assay and qPCR quantification**

749

750 ChIP assay was performed as mentioned previously (Fangaria et al., 2022; Kumar et al., 2021;
751 Makrantoni et al., 2019; Mehta et al., 2014). First, cells were grown in the presence of 3%
752 glycerol till 0.3 OD. A total of 60 OD cells were harvested (0 h), and the remaining cells were
753 treated with 3% galactose. A total of 60 OD of cells were harvested every hr till 4 hrs. The cells
754 were then fixed with 1% formaldehyde for 30 mins at 25°C at 100 rpm, followed by quenching

755 by the addition of glycine at a final concentration of 125 mM. The cells were then harvested
756 and washed twice in ice-cold TBS buffer (20 mM Tris–HCl pH 7.5, 150 mM NaCl) and once
757 with 10 ml of FA lysis buffer (50 mM Hepes–KOH pH 7.5, 150 mM NaCl, 1 mM EDTA, 1%
758 Triton X-100, 0.1% Na-deoxycholate) supplemented with 0.1 % SDS. The pellet was
759 resuspended in 500 µl of 1X FA lysis buffer supplemented with 0.5% SDS, 1 mM PMSF, 1X
760 PIC. The cells were lysed using 0.5 mm glass beads using a mini-bead beater (BIOSPEC,
761 India) for 7 cycles (1 min ON, 2 mins OFF on ice). The lysate was collected in a pre-chilled
762 1.5 ml eppendorf tube and centrifuged twice at 16,000 x g for 15 mins at 4°C. The pellet was
763 resuspended in 300 µl ice-cold 1X FA lysis buffer supplemented with 0.1% SDS, 1 mM PMSF,
764 and 1X PIC. The chromatin was then sheared to 200-600 bps using a water bath sonicator
765 (Diagenode SA, Picoruptor, BC 100,27 LAUDA Germany) for 30 cycles of 30 s ON / 30 s OFF
766 at 4°C. After clarification of the lysate by centrifugation at 16,000 x g for 10 mins at 4°C, 3-5
767 µg of appropriate antibodies (were added and incubated at 4°C overnight with gentle rotation.
768 Subsequently, 50 µl Protein-A conjugated Sepharose beads were added and incubated for 2
769 h at 4°C with rotation. The beads were washed twice with IP wash buffer I (1X FA lysis buffer,
770 0.1%SDS, 275 mM NaCl), followed by one wash in IP wash buffer II (1X FA lysis buffer,
771 0.1%SDS, 500 mM NaCl, III (10 mM Tris pH 8.0, 250 mM LiCl, 0.5% NP-40, 0.5% sodium
772 deoxycholate, 1 mM EDTA), and 1X TE at room temperature The beads were resuspended
773 in elution buffer and the chromatin was eluted by boiling at 65°C. The eluate was then
774 decrosslinked overnight at 65°C, followed by Proteinase K (SRL, India) treatment for 2 hrs at
775 45°C. The DNA was purified by PCI-based purification and precipitated overnight in chilled
776 ethanol at -80°C. The enrichment of obtained chromatin fragments was estimated using qPCR
777 (BioRad CFX96, USA) using specific primers targeting specific and non-specific (negative
778 control) chromatin loci, listed in Table S2. As mentioned before (Kumar et al., 2021; Shah et
779 al., 2023) the following equation was used to estimate the percentage of chromatin
780 enrichment. ChIP efficiency = Enrichment/Input X 100; Enrichment/Input = E^-ΔCT;
781 ΔCT = CT(ChIP) − [CT(Input) − LogEX(D)]; E = primer efficiency value, CT = Threshold values
782 obtained from qPCR, D = Input dilution factor. E was estimated as {[10^(-1/slope)]– 1} from
783 standardization graphs of CT values against dilutions of the input DNA.
784
785 **Chromatin immunoprecipitation (ChIP) and sequencing**
786
787 ChIP assay was performed as mentioned above with certain modifications. The cells were
788 grown till mid-log and treated with nocodazole (20 ug/ml) for 90 mins to arrest cells at
789 metaphase and were subsequently treated with 0.05% MMS for additional 90 mins. The cells
790 were harvested and processed for immunoprecipitation, as mentioned above except Protein-
791 A conjugated dyna beads were used instead of sepharose beads. 10 ng of DNA eluate was

792 taken to prepare the NGS library using a TruSeq ChIP sample preparation kit from Illumina.
793 The library was prepared as per the manufacturer's protocol. Library QC was performed by
794 measuring the concentration and size of the libraries by using the 4150 Tapestation system
795 from Agilent and Qubit dsDNA HS assay kit (Thermo Fisher Scientific). The libraries were
796 sequenced using the Illumina platform in paired-end mode with a read length of 151 bp by
797 Macrogen Asia Pacific Pte. Ltd, Singapore.
798
799 **Bioinformatics analysis**
800 The ChIP-Seq analysis was performed by Genotypic (Bengaluru,India). The raw reads were
801 processed using FastQC (Andrews S., 2010) for quality assessment and pre-processing,
802 which includes removing the adapter sequences and low quality bases (<q30) using
803 TrimGalore (Krueger F., 2015). The pre-processed high quality read data was aligned to
804 reference *Saccharomyces cerevisiae* genome data base using Bowtie**,** which is an ultrafast,
805 memory-efficient short read aligner geared towards quickly aligning large sets of short DNA
806 sequences (reads) to large genomes. The aligned files (BAM files) were used for peak calling
807 using MACS2 software with input sample as a control. The bedgraph files generated from
808 MACS2 software were used to plot the graphs using the IGV browser (Robinson et al., 2011).
809
810 **Protein extraction, gel running and western blotting**
811
812 Yeast cells harvested at the mentioned time points were washed once with ice-cold water and
813 once with ice-cold 20% TCA. To preserve the phosphorylation moieties, the cells were lysed
814 in the presence of 1X PhosSTOP (Roche). The pellet was resuspended in 200 µl of 20% TCA,
815 and an equal volume of glass beads was added, and cells were lysed using a mini bead beater
816 (BIOSPEC, India) for 7 cycles (1 min ON, 2 mins OFF on ice). The supernatant was collected
817 after puncturing the O-ring tube and centrifugating at 2800 rpm for 2 mins at 4°C. 400 µl of 5%
818 TCA was added to the beads and spun again to collect the supernatant. The total supernatant
819 was spun at maximum speed for 10 mins at 4°C. The precipitate was kept for air-drying for
820 10-15 mins before resuspending in 2X SDS sample buffer and 1X Tris (pH 8.0) for
821 neutralization. Before loading, the protein was boiled for 5 mins at 95°C and spun at maximum
822 speed for 30 seconds. Standard procedure was followed for SDS-PAGE and western blot
823 transfer.
824 For the gel containing the PhosTag reagent, 10 mM $MnCl_2$ was added to the resolving
825 gel along with 50 µM of the PhosTag reagent (AAL-107, FUJIFILM, JAPAN). Before western
826 blotting, the gel was washed three times with 1 mM EDTA for 10 mins, followed by 2 washes
827 in transfer buffer. The blot was further incubated with primary antibodies at a dilution of 1:2500,
828 while the secondary antibodies were used at 1:5000 dilution.

829 **Statistical analyses**

830

831 The data presented in the main figures and the supplementary figures were obtained from two
832 to three independent experiments. The error bars in the individual bar graphs represent the
833 standard error (SE) derived from the standard deviation (SD). The statistical significance (*p*)
834 was determined by two-tailed Student's t-test, or one-way ANOVA test, as appropriate. When
835 comparing more than one group, a one-way ANOVA test was used; otherwise, Student's t-
836 test was used. The 'N' values denote the total number of cells analyzed from the combined 'n'
837 number of replicates of the individual assays. The *p* values less than or equal to 0.05 are
838 categorized as significant differences. The SD, SE, and statistical significance (*p*) values were
839 calculated using automated modules of GraphPad Prism 9.0 (Version 9.4.1) software.

840

841 **Figures**

842

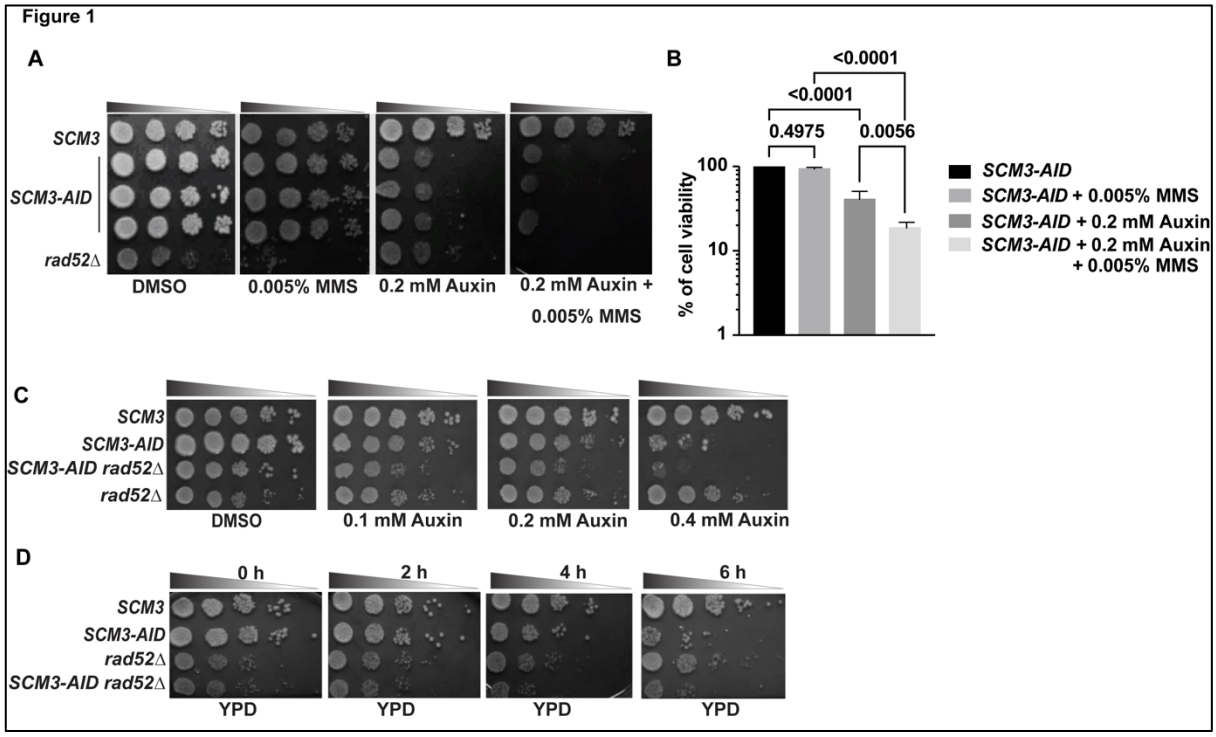

843

844 **Figure 1. Loss of Scm3 causes sensitivity to MMS-mediated DNA damage. (A)** Wild-type
845 (*SCM3*), *SCM3-AID* (three independent transformants)*, and rad52*Δ cells grown till mid-log
846 were serially diluted and spotted on the indicated plates. The plates were incubated at 30°C
847 for 24-48 hrs before imaging. **(B)** An equal number of mid-log grown *SCM3-AID* cells were
848 spread on plates containing indicated supplements. From the number of colonies that
849 appeared after incubation at 30°C for 2 days, the cell viability was estimated (see materials
850 and methods) and plotted. Colonies formed on the plate without auxin and MMS were taken
851 as 100% viability, and accordingly, viability percentage was calculated for other plates. The *p*
852 values were estimated by one-way ANOVA test from three independent experiments. **(C)** Wild-
853 type (*SCM3)*, *SCM3-AID, SCM3-AID rad52*Δ*,* and *rad52*Δ cells grown till mid-log were serially

854 diluted and spotted in the presence of indicated auxin concentrations. The plates were
855 incubated at 30°C for 24-48 hrs before imaging. **(D)** The cells of the strains used in (C) were
856 grown till mid-log and treated with 0.75 mM auxin for the indicated duration before they were
857 washed, serially diluted, and spotted on YPD plates that were incubated at 30°C for 24-48 hrs
858 before imaging.

859

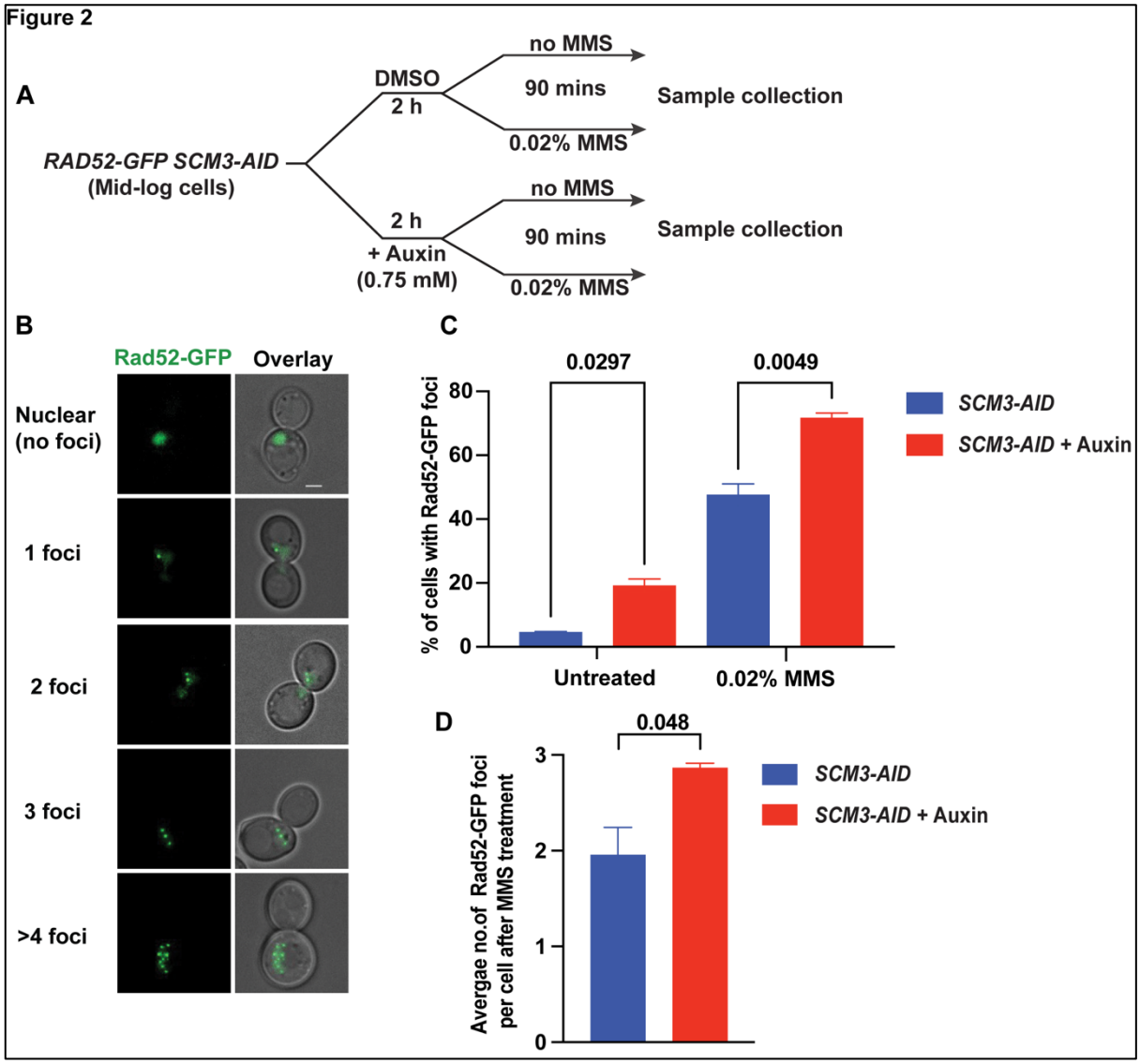

860

861 **Figure 2. Loss of Scm3 causes increased Rad52 foci in the presence or absence of**
862 **MMS. (A)** The schematic of the experimental strategy that was followed for visualization of
863 Rad52-GFP foci in the *RAD52-GFP SCM3-AID* cells either in the presence of DMSO (wild-
864 type) or auxin (Scm3 depleted) and each either treated with MMS or left untreated. **(B)**
865 Representative images showing different patterns of Rad52-GFP foci. Rad52-GFP produces
866 a nuclear signal (row 1) in the absence of any DNA damage, but with the damage, it coalesces
867 to form bright foci (rows 2-5) representing the DNA repair sites. **(C)** The percentage of
868 indicated cells containing Rad52-GFP foci with or without MMS treatment for 90 mins. **(D)** The
869 average number of Rad52-GFP foci per MMS-treated cell from the experiment described in
870 (C). At least 300 cells were analyzed from three independent experiments for each set in **(C)**

and **(D)**. The *p* values were estimated by unpaired two-tailed student's t-test. Scale bar = 2 µm.

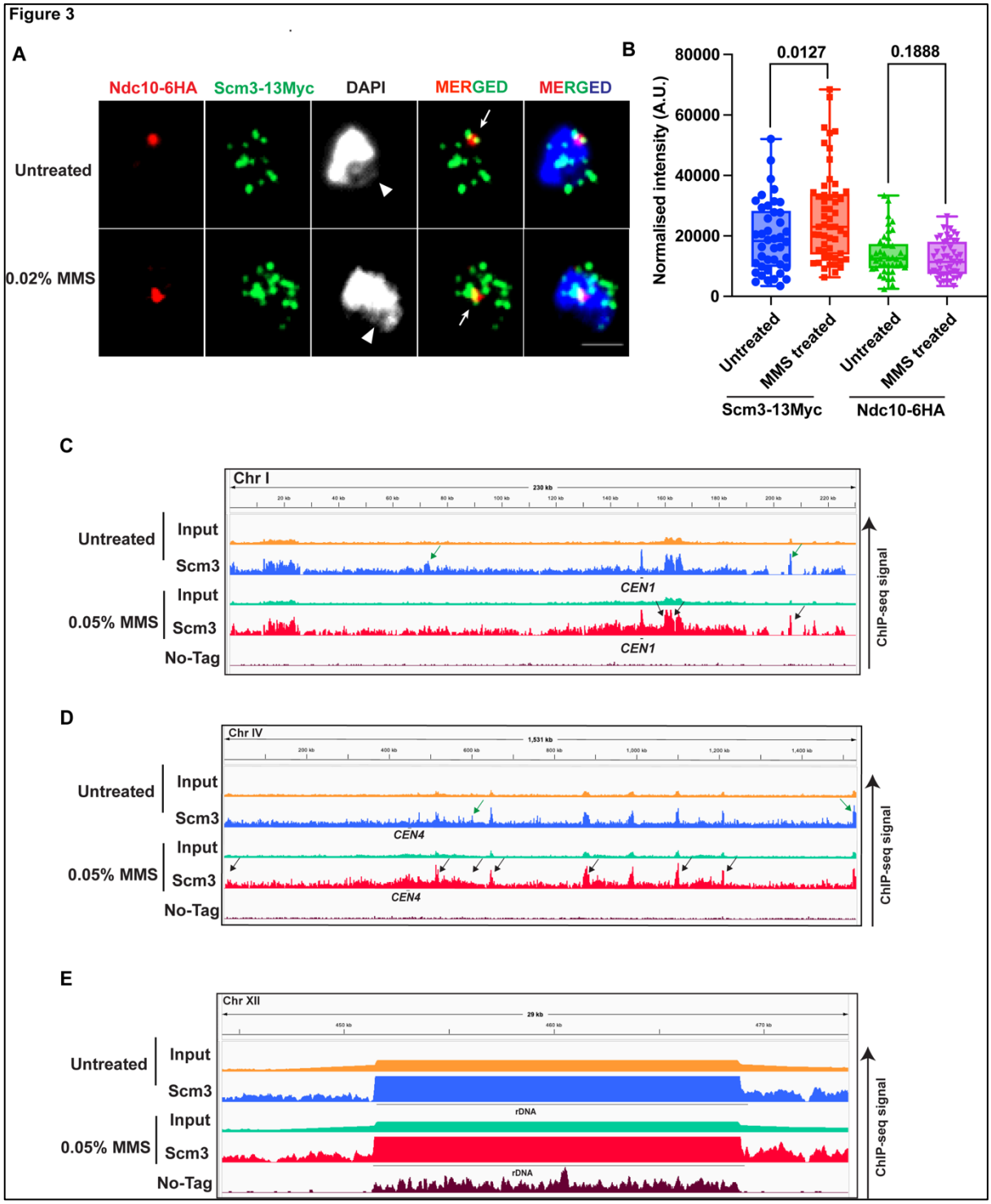

Figure 3. The localization of Scm3 in response to DNA damage. (A) Representative images showing the localizations of Ndc10-6HA and Scm3-13Myc using chromatin spread. The mid-log grown *NDC10-6HA SCM3-13MYC* cells were treated with 0.02% MMS or mock-treated for 90 mins for the assay. The arrow shows the co-localization of Ndc10-6HA and Scm3-13Myc at the kinetochore cluster, and the arrowhead shows the rDNA loop. **(B)** The intensities of Scm3-13Myc and Ndc10-6HA normalized with the background intensity were

quantified using ImageJ software and were plotted. At least 30 spreads from 2 independent experiments were analyzed for each set in **(B).** The *p* values were estimated by unpaired two-tailed student's t-test. Scale bar = 2 µm. **(C, D)** The ChIP-seq signal of Scm3 (Scm3-13Myc) and input from cells either untreated or treated with 0.05% MMS for the entire chromosome I; the no-tag strain was used as a control. The plot shows the binding of Scm3 across (C) chromosome I and (D) chromosome IV. The green and black arrows represent the non-centromeric localization of Scm3 in untreated, and MMS treated samples, respectively. **(E)** Same as (C); only a portion of chromosome XII flanking 9.1 kb rDNA region is shown. The scale is 7–50 for the input samples and 7-25 for IP samples.

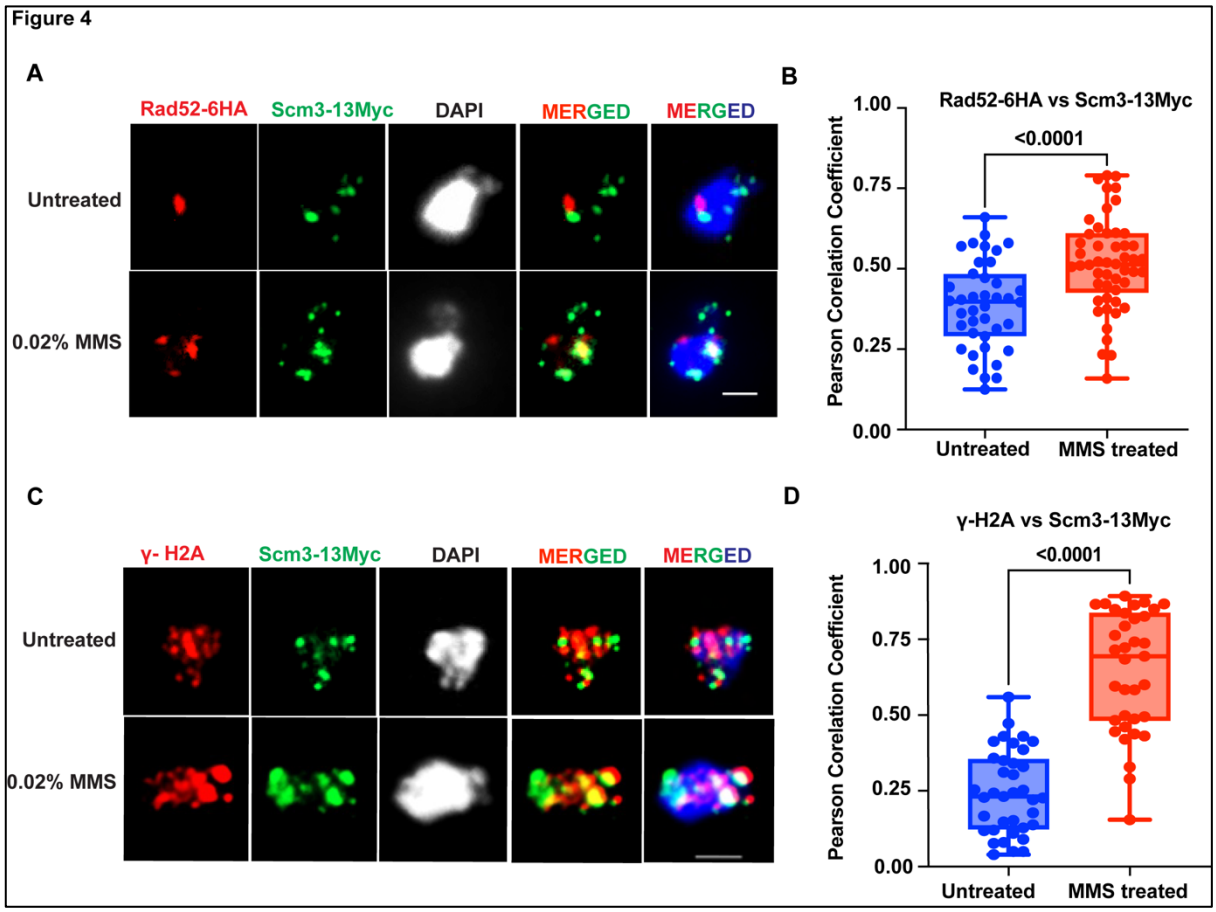

Figure 4. Scm3 colocalizes with DDR proteins in response to DNA damage. (A) Representative images showing the localizations of Rad52-6HA and Scm3-13Myc using chromatin spread. The mid-log grown *RAD52-6HA SCM3-13MYC* cells were treated with 0.02% MMS or mock-treated for 90 mins for the assay. **(B)** The quantification of the colocalization between Rad52-6HA and Scm3-13Myc was calculated using Pearson's correlation coefficient (PCC). **(C)** Representative images showing the localizations of γ-H2A and Scm3-13Myc using chromatin spread. The mid-log grown *SCM3-MYC* cells were treated with 0.02% MMS or mock-treated for 90 mins for the assay. **(D)** The quantification of the colocalization between γ-H2A and Scm3-13Myc was calculated using PCC. Anti-HA (12CA5, Roche), anti-Myc (9E10, Roche), and anti-H2A (ab15083, Abcam) antibodies were used to detect HA, Myc, and H2A-S129, respectively. At least 30 spreads from 2 independent

907 experiments were analyzed for each set in **(B),** and **(D)**. The *p* values were estimated by
908 unpaired two-tailed student's t-test. Scale bar = 2 μm.
909

Figure 5

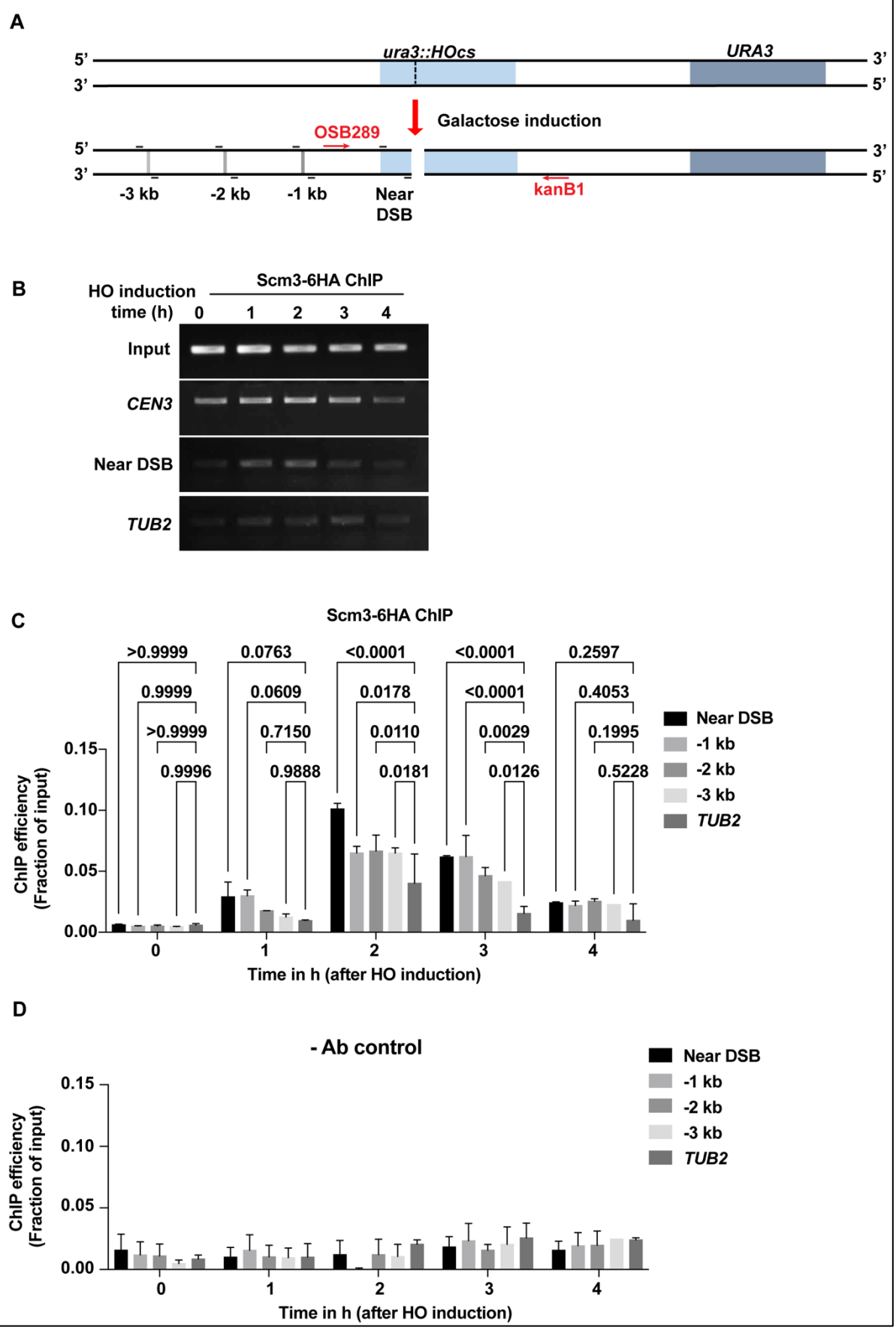
A
ura3::HOcs
URA3
5'
3'
3'
5'
Galactose induction
OSB289
5'
3'
3'
5'
-3 kb
-2 kb
-1 kb
Near DSB
kanB1
B
HO induction time (h)
Scm3-6HA ChIP
0
1
2
3
4
Input
CEN3
Near DSB
TUB2
C
Scm3-6HA ChIP
>0.9999
0.9999
>0.9999
0.9996
0.0763
0.0609
0.7150
0.9888
<0.0001
0.0178
0.0110
0.0181
<0.0001
<0.0001
0.0029
0.0126
0.2597
0.4053
0.1995
0.5228
Near DSB
-1 kb
-2 kb
-3 kb
TUB2
ChIP efficiency (Fraction of input)
0.15
0.10
0.05
0.00
0
1
2
3
4
Time in h (after HO induction)
D
- Ab control
Near DSB
-1 kb
-2 kb
-3 kb
TUB2
ChIP efficiency (Fraction of input)
0.15
0.10
0.05
0.00
0
1
2
3
4
Time in h (after HO induction)

910

Figure 5. Scm3 is recruited to a site-specific double-stranded break (DSB). (A) Schematic representation of a cut site of the *HO* endonuclease (*HOcs*) integrated at the *URA3* locus in the NA14 strain. Upon galactose induction, the *HO* endonuclease cleaves the DNA at the specific site generating DSB. The positions of the primers (OSB289 and kanB1) are shown that were used to detect the DSB, and the binding of Scm3 near and distal (-1 to -3 kb) to the DSB **(B)** ChIP analyses were performed to quantify the association of Scm3-6HA in NA14 strain harboring *SCM3-6HA* with the indicated loci at the indicated time points. The PCR amplified DNA bands following ChIP were run on agarose gel and stained with ethidium bromide. **(C)** ChIP analyses for measuring the association of Scm3-6HA with the indicated loci were performed at the indicated time points of HO induction using anti-HA (12CA5, Roche) antibodies. The ChIP efficiency as percentage enrichment per input obtained by qPCR analysis of the immunoprecipitated DNA was plotted. **(D)** Same analysis as in (C) using no antibody (-Ab) control. The *p* values in **(C)** and **(D)** were estimated from two independent experiments.

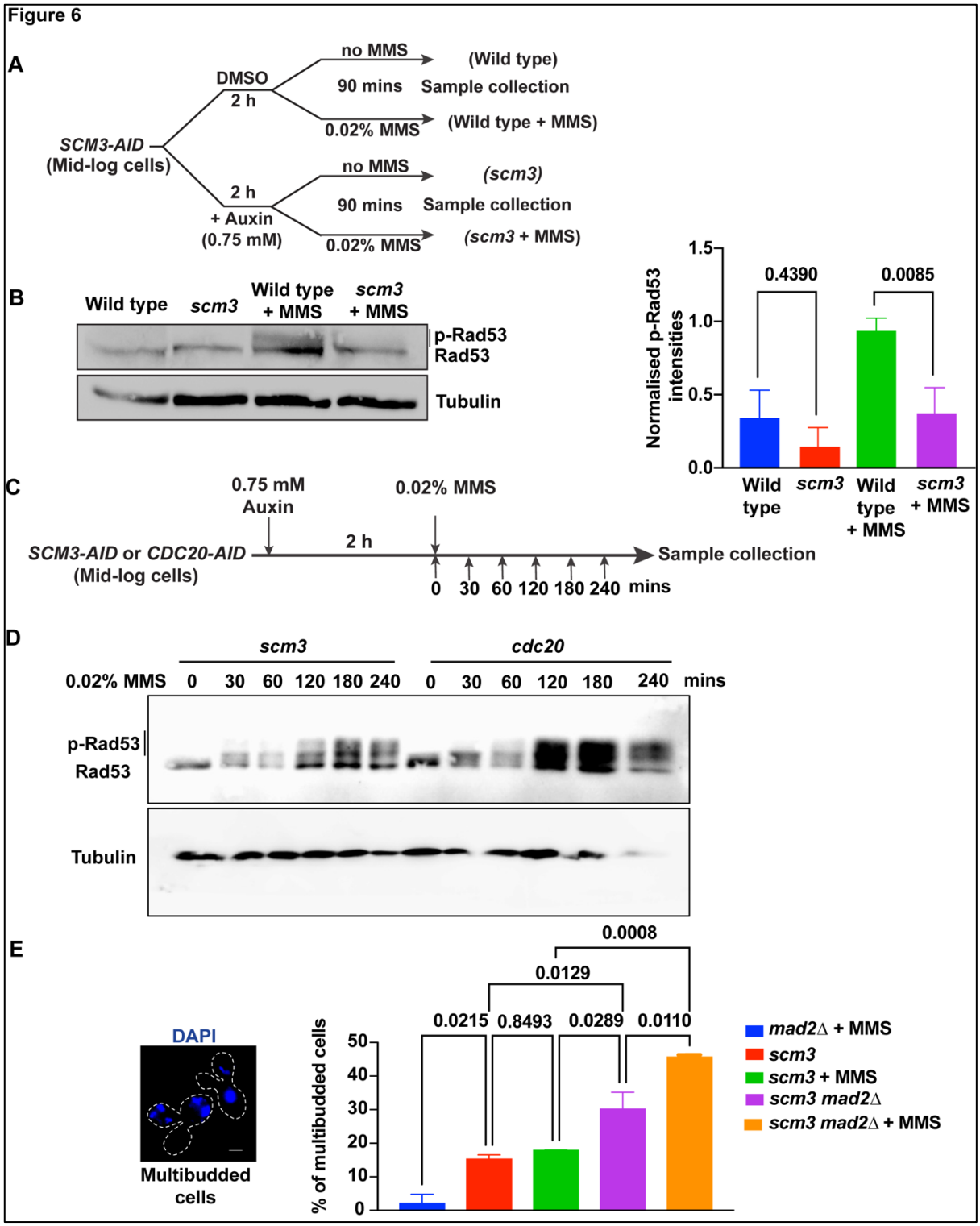

927

928 **Figure 6. Evidence of improper activation of DNA damage checkpoint in absence of**
929 **Scm3. (A)** The schematic of the experimental strategy that was followed for detecting Rad53
930 in *SCM3-AID* cells in the presence of DMSO (wild-type) or auxin (Scm3 depleted) and each
931 either treated with MMS or left untreated. **(B)** Left**,** western blots showing p-Rad53/Rad53 and
932 tubulin (as loading control) using anti-Rad53 (ab104232, Abcam) and anti-tubulin (MCA78G,
933 Serotec) antibodies, respectively, from indicated cells obtained from (A). Right, the intensities
934 of the p-Rad53 measured by ImageJ were plotted after normalizing with the corresponding
935 loading control. **(C)** The schematic of the experimental strategy to detect Rad53 in Scm3 or

936 Cdc20 depleted cells treated with MMS for different time points. **(D)** Western blots developed
937 as in **(**B) from indicated cells obtained from (**C**). **(E)** *mad2*Δ*, SCM3-AID,* and *SCM3-AID mad2*Δ
938 cells were first treated with 0.75 mM auxin for 2 hrs to deplete Scm3 and then either treated
939 with 0.02% MMS for 90 mins or left untreated. The cells were harvested and were scored for
940 the presence of multibudded cells (shown on the left). At least 150 cells from three
941 independent experiments were analyzed for each set**.** The *p* values were estimated by one-
942 way ANOVA test. Scale bar = 2 µm.

943

944

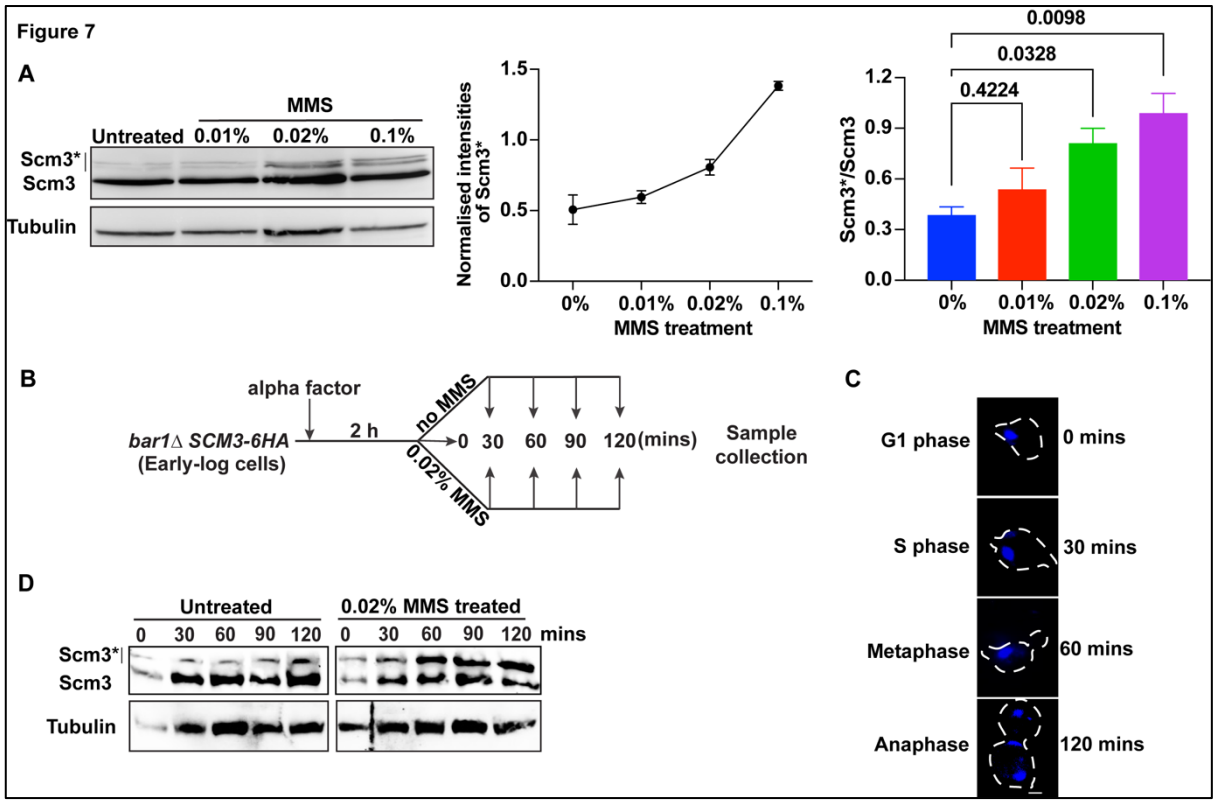

945

946

947 **Figure 7. Post-translational modification of Scm3 in response to DNA damage (A)** Left,
948 western blots show Scm3-6HA and its modified form (Scm3*) along with tubulin as loading
949 control from the cells untreated or treated with indicated concentrations of MMS for 90 mins.
950 The cell lysates were probed using anti-HA (12CA5, Roche) or anti-tubulin (MCA78G, Serotec)
951 antibodies. Middle, the graph shows the intensity of Scm3* with increasing MMS
952 concentrations, normalized with respect to tubulin using ImageJ software. Right, the graph
953 represents the ratio of the modified to unmodified forms of Scm3. **(B)** The schematic of the
954 experimental strategy that was followed for detecting Scm3-6HA in the G1 arrested cells and
955 following their release from the arrest for the indicated time in the absence or presence of
956 MMS. **(C)** Representative images showing the cell cycle stages by DAPI staining and bud
957 morphology at indicated time points since their release from G1 arrest. **(D)** Western blot
958 showing Scm3-6HA along with tubulin as a loading control from the cells harvested, as shown

in (B). The cell lysates were probed using anti-HA and anti-tubulin antibodies to detect Scm3-6HA and tubulin, respectively. Error bars represent the standard deviation from mean values obtained from two independent experiments. Scale bar = 2 µm.

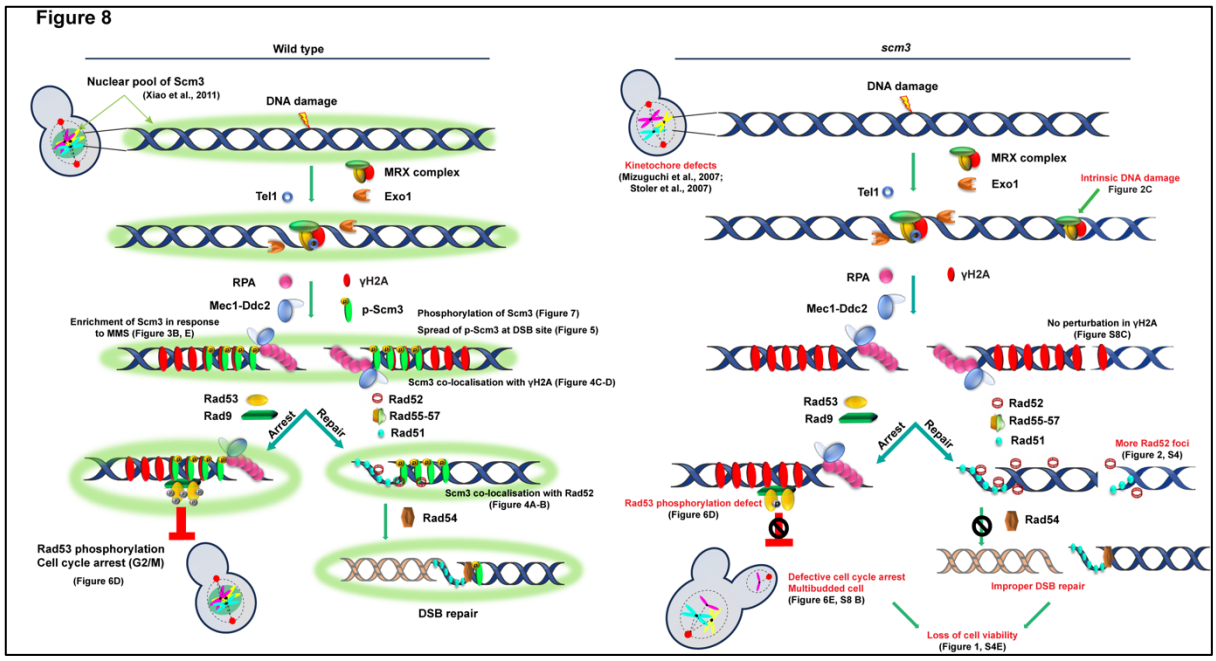

Figure 8: A working model summarizing the role of Scm3 in DNA damage response (DDR). Left, in wild type cells, a subset of the Scm3 molecules present as a nuclear pool (green) are phosphorylated upon DNA damage. The phosphorylated Scm3 (p-Scm3) associates with DSB sites, colocalizes with yH2A, and spreads to the chromatin, flanking the DSB site. Possibly, the p-Scm3 facilitates proper activation of Rad53 through its phosphorylation, leading to cell cycle arrest. Additionally, p-Scm3 co-localizes with Rad52 and assists in DSB repair. Right, in *scm3* mutant cells, there is also an increase in intrinsic DNA damage, corresponding to more Rad52 foci formation, and due to the inability to repair DSBs, the cell viability drops. In parallel, reduced Rad53 activation causes improper DDR-mediated cell cycle arrest generating multibudded cells and aneuploids which causes cell death. The phenotypes associated with the loss of Scm3 are shown in red.

References

1. Agmon N, Pur S, Liefshitz B, Kupiec M. 2009. Analysis of repair mechanism choice during homologous recombination. *Nucleic Acids Res* **37**:5081–5092. doi:10.1093/NAR/GKP495
2. Amon A. 2002. Synchronization procedures. pp. 457–467. doi:10.1016/S0076-6879(02)51864-4
3. Andrews, S., 2010. FastQC: a quality control tool for high throughput sequence data.
4. Aravind L, Iyer LM, Wu C. 2007. Domain architectures of the Scm3p protein provide insights into centromere function and evolution. *Cell Cycle* **6**:2511–2515. doi:10.4161/CC.6.20.4793
5. Barlow JH, Rothstein R. 2010. Timing is everything: cell cycle control of Rad52. *Cell Div* **5**:7. doi:10.1186/1747-1028-5-7

6. Blower MD, Karpen GH. 2001. The role of Drosophila CID in kinetochore formation, cell-cycle progression and heterochromatin interactions. *Nat Cell Biol* **3**:730–739. doi:10.1038/35087045
7. Buchwitz BJ, Ahmad K, Moore LL, Roth MB, Henikoff S. 1999. A histone-H3-like protein in C. elegans. *Nature* **401**:547–548. doi:10.1038/44062
8. Burgess RJ, Zhang Z. 2013. Histone chaperones in nucleosome assembly and human disease. *Nat Struct Mol Biol* **20**:14. doi:10.1038/NSMB.2461
9. Burma S, Chen BP, Murphy M, Kurimasa A, Chen DJ. 2001. ATM Phosphorylates Histone H2AX in Response to DNA Double-strand Breaks. *Journal of Biological Chemistry* **276**:42462–42467. doi:10.1074/jbc.C100466200
10. Camahort R, Li B, Florens L, Swanson SK, Washburn MP, Gerton JL. 2007. Scm3 Is Essential to Recruit the Histone H3 Variant Cse4 to Centromeres and to Maintain a Functional Kinetochore. *Mol Cell* **26**:853–865. doi:10.1016/J.MOLCEL.2007.05.013
11. Chen T, Huang H, Zhou Y, Geng L, Shen T, Yin S, Zhou L, Zheng S. 2018. HJURP promotes hepatocellular carcinoma proliferation by destabilizing p21 via the MAPK/ERK1/2 and AKT/GSK3β signaling pathways. *Journal of Experimental and Clinical Cancer Research* **37**. doi:10.1186/s13046-018-0866-4
12. Chen Y, Baker RE, Keith KC, Harris K, Stoler S, Fitzgerald-Hayes M. 2000. The N Terminus of the Centromere H3-Like Protein Cse4p Performs an Essential Function Distinct from That of the Histone Fold Domain. *Mol Cell Biol* **20**:7037. doi:10.1128/MCB.20.18.7037-7048.2000
13. Cho US, Harrison SC. 2012. Ndc10 is a platform for inner kinetochore assembly in budding yeast. *Nat Struct Mol Biol* **19**:48–56. doi:10.1038/NSMB.2178
14. Cho US, Harrison SC. 2011. Recognition of the centromere-specific histone Cse4 by the chaperone Scm3. *Proc Natl Acad Sci U S A* **108**:9367–9371. doi:10.1073/PNAS.1106389108
15. Choy JS, Mishra PK, Au WC, Basrai MA. 2012. Insights into assembly and regulation of centromeric chromatin in Saccharomyces cerevisiae. *Biochim Biophys Acta Gene Regul Mech* **1819**:776–783. doi:10.1016/J.BBAGRM.2012.02.008
16. Ciccia A, Elledge SJ. 2010. The DNA Damage Response: Making It Safe to Play with Knives. *Mol Cell*. doi:10.1016/j.molcel.2010.09.019
17. Coates P, Dewar J, Thompson AM. 2010. At last, a predictive and prognostic marker for radiotherapy? *Breast Cancer Res* **12**:106. doi:10.1186/BCR2567
18. Conde F, San-Segundo PA. 2008. Role of Dot1 in the Response to Alkylating DNA Damage in Saccharomyces cerevisiae: Regulation of DNA Damage Tolerance by the Error-Prone Polymerases Polζ/Rev1. *Genetics* **179**:1197. doi:10.1534/GENETICS.108.089003
19. Dammann R, Lucchini R, Koller T, Sogo JM. 1993. Chromatin structures and transcription of rDNA in yeast Saccharomyces cerevisiae. *Nucleic Acids Res* **21**:2331. doi:10.1093/NAR/21.10.2331
20. De Koning L, Corpet A, Haber JE, Almouzni G. 2007. Histone chaperones: an escort network regulating histone traffic. *Nat Struct Mol Biol* **14**:997–1007. doi:10.1038/nsmb1318
21. Dornfeld KJ, Livingston DM. 1991. Effects of controlled RAD52 expression on repair and recombination in Saccharomyces cerevisiae. *Mol Cell Biol* **11**:2013–2017. doi:10.1128/MCB.11.4.2013-2017.1991
22. Dou Z, Qiu C, Zhang X, Yao S, Zhao C, Wang Z, Chu R, Chen J, Chen Z, Li R, Wang K, Liu P, Liu C, Song K, Kong B. 2022. HJURP Promotes Malignant Progression and Mediates Sensitivity to Cisplatin and WEE1-inhibitor in Serous Ovarian Cancer. *Int J Biol Sci* **18**:1188–1210. doi:10.7150/ijbs.65589
23. Dunleavy EM, Roche D, Tagami H, Lacoste N, Ray-Gallet D, Nakamura Y, Daigo Y, Nakatani Y, Almouzni-Pettinotti G. 2009. HJURP is a cell-cycle-dependent maintenance and deposition factor of CENP-A at centromeres. *Cell* **137**:485–497. doi:10.1016/J.CELL.2009.02.040

24. Earnshaw WC, Rothfield N. 1985. Identification of a family of human centromere proteins using autoimmune sera from patients with scleroderma. *Chromosoma 1985 91:3* **91**:313–321. doi:10.1007/BF00328227
25. Earnshaw WC, Tomkiel JE. 1992. Centromere and kinetochore structure. *Curr Opin Cell Biol* **4**:86–93. doi:10.1016/0955-0674(92)90063-I
26. Eitoku M, Sato L, Senda T, Horikoshi M. 2008. Histone chaperones: 30 years from isolation to elucidation of the mechanisms of nucleosome assembly and disassembly. *Cellular and Molecular Life Sciences* **65**:414–444. doi:10.1007/s00018-007-7305-6
27. Fan J, Moreno AT, Baier AS, Loparo JJ, Peterson CL. 2022. H2A.Z deposition by SWR1C involves multiple ATP-dependent steps. *Nat Commun* **13**:7052. doi:10.1038/s41467-022-34861-x
28. Fangaria N, Rani K, Singh P, Dey S, Kumar KA, Bhattacharyya S. 2022. DNA damage-induced nuclear import of HSP90α is promoted by Aha1. *Mol Biol Cell* **33**. doi:10.1091/MBC.E21-11-0554
29. Fischböck-Halwachs J, Singh S, Potocnjak M, Hagemann G, Solis-Mezarino V, Woike S, Ghodgaonkar-Steger M, Weissmann F, Gallego LD, Rojas J, Andreani J, Köhler A, Herzog F. 2019. The COMA complex interacts with Cse4 and positions Sli15/ipl1 at the budding yeast inner kinetochore. *Elife* **8**. doi:10.7554/ELIFE.42879
30. Foltz DR, Jansen LET, Bailey AO, Yates JR, Bassett EA, Wood S, Black BE, Cleveland DW. 2009. Centromere-Specific Assembly of CENP-A Nucleosomes Is Mediated by HJURP. *Cell* **137**:472–484. doi:10.1016/j.cell.2009.02.039
31. Foltz DR, Jansen LET, Black BE, Bailey AO, Yates JR, Cleveland DW. 2006. The human CENP-A centromeric nucleosome-associated complex. *Nat Cell Biol* **8**:458–469. doi:10.1038/NCB1397
32. Giaimo BD, Ferrante F, Herchenröther A, Hake SB, Borggrefe T. 2019. The histone variant H2A.Z in gene regulation. *Epigenetics Chromatin* **12**:37. doi:10.1186/s13072-019-0274-9
33. Daniel Gietz, R., & Woods, R. A. (2002). Transformation of yeast by lithium acetate/single-stranded carrier DNA/polyethylene glycol method (pp. 87–96). https://doi.org/10.1016/S0076-6879(02)50957-5
34. Gilbert CS, Green CM, Lowndes NF. 2001. Budding Yeast Rad9 Is an ATP-Dependent Rad53 Activating Machine. *Mol Cell* **8**:129–136. doi:10.1016/S1097-2765(01)00267-2
35. Haber JE. 2018. DNA repair: the search for homology. *Bioessays* **40**:e1700229. doi:10.1002/BIES.201700229
36. Hallwyl SCL, Shi I, Krejci L, Mü Ller ‡ C, Albertsen L, Sung P, Mortensen UH. 2008. Interaction with RPA Is Necessary for Rad52 Repair Center Formation and for Its Mediator Activity * □ S Iben Plate ‡1. doi:10.1074/jbc.M804881200
37. Hammond CM, Strømme CB, Huang H, Patel DJ, Groth A. 2017. Histone chaperone networks shaping chromatin function. *Nature Reviews Molecular Cell Biology 2017 18:3* **18**:141–158. doi:10.1038/nrm.2016.159
38. Hoffman CS. 1997. Preparation of Yeast DNA. *Curr Protoc Mol Biol* **39**. doi:10.1002/0471142727.mb1311s39
39. Howman E V., Fowler KJ, Newson AJ, Redward S, MacDonald AC, Kalitsis P, Choo KHA. 2000. Early disruption of centromeric chromatin organization in centromere protein A (*Cenpa*) null mice. *Proceedings of the National Academy of Sciences* **97**:1148–1153. doi:10.1073/pnas.97.3.1148
40. Hu B, Wang Q, Wang Y, Chen J, Li P, Han M. 2017. Holliday junction–recognizing protein promotes cell proliferation and correlates with unfavorable clinical outcome of hepatocellular carcinoma. *Onco Targets Ther* **10**:2601–2607. doi:10.2147/OTT.S127738
41. Hu Z, Huang G, Sadanandam A, Gu S, Lenburg ME, Pai M, Bayani N, Blakely EA, Gray JW, Mao JH. 2010. The expression level of HJURP has an independent prognostic impact and predicts the sensitivity to radiotherapy in breast cancer. *Breast Cancer Research* **12**. doi:10.1186/BCR2487
42. Janke C, Magiera MM, Rathfelder N, Taxis C, Reber S, Maekawa H, Moreno-Borchart A, Doenges G, Schwob E, Schiebel E, Knop M. 2004. A versatile toolbox for PCR-based

1097 tagging of yeast genes: new fluorescent proteins, more markers and promoter substitution
1098 cassettes. *Yeast* **21**:947–962. doi:10.1002/yea.1142
1099 43. Javaheri A, Wysocki R, Jobin-Robitaille O, Altaf M, Cô Té § J, Kron SJ. 2006. Yeast G1
1100 DNA damage checkpoint regulation by H2A phosphorylation is independent of chromatin
1101 remodeling.
1102 44. Kang DH, Woo J, Kim H, Kim SY, Ji S, Jaygal G, Ahn TS, Kim HJ, Kwak HJ, Kim CJ, Baek
1103 MJ, Jeong D. 2020. Prognostic relevance of hjurp expression in patients with surgically
1104 resected colorectal cancer. *Int J Mol Sci* **21**:1–12. doi:10.3390/ijms21217928
1105 45. Kato T, Sato N, Hayama S, Yamabuki T, Ito T, Miyamoto M, Kondo S, Nakamura Y, Daigo
1106 Y. 2007. Activation of Holliday junction-recognizing protein involved in the chromosomal
1107 stability and immortality of cancer cells. *Cancer Res* **67**:8544–8553. doi:10.1158/0008-
1108 5472.
1109 46. Kaytor MD, Livingston DM. 1994. Saccharomyces cerevisiae RAD52 Alleles Temperature-
1110 Sensitive for the Repair of DNA Double-Strand Breaks.
1111 47. Kirkland JG, Peterson MR, Still Ii CD, Brueggeman L, Dhillon N, Kamakaka RT. 2015.
1112 Heterochromatin formation via recruitment of DNA repair proteins **26**.
1113 doi:10.1091/mbc.E14-09-1413
1114 48. Kitada T, Schleker T, Sperling AS, Xie W, Gasser SM, Grunstein M. 2011. Cell Cycle γH2A
1115 is a component of yeast heterochromatin required for telomere elongation View
1116 supplementary material. *www.landesbioscience.com Cell Cycle* **293**:293–300.
1117 doi:10.4161/cc.10.2.14536
1118 49. Kumar D, Prajapati HK, Mahilkar A, Ma C-H, Mittal P, Jayaram M, Ghosh SK. 2021. The
1119 selfish yeast plasmid utilizes the condensin complex and condensed chromatin for faithful
1120 partitioning. *PLoS Genet* **17**:e1009660. doi:10.1371/journal.pgen.1009660
1121 50. Krueger F. 2015. Trim Galore: a wrapper tool around Cutadapt and FastQC to consistently
1122 apply quality and adapter trimming to FastQ
1123 files. http://www.bioinformatics.babraham.ac.uk/projects/trim_galore.
1124 51. Lai W, Zhu W, Xiao C, Li X, Wang Y, Han Y, Zheng J, Li Y, Li M, Wen X. 2021. HJURP
1125 promotes proliferation in prostate cancer cells through increasing CDKN1A degradation
1126 via the GSK3β/JNK signaling pathway. *Cell Death Dis* **12**. doi:10.1038/s41419-021-03870-
1127 x
1128 52. Lang J, Barber A, Biggins S. 2018. An assay for de novo kinetochore assembly reveals a
1129 key role for the CENP-T pathway in budding yeast. *Elife* **7**. doi:10.7554/eLife.37819
1130 53. Lanz MC, Yugandhar K, Gupta S, Sanford EJ, Faça VM, Vega S, Joiner AMN, Fromme
1131 JC, Yu H, Smolka MB. 2021. In-depth and 3-dimensional exploration of the budding yeast
1132 phosphoproteome. *EMBO Rep* **22**. doi:10.15252/EMBR.202051121
1133 54. Lee C-S, Lee K, Legube G, Haber JE. 2014. Dynamics of yeast histone H2A and H2B
1134 phosphorylation in response to a double-strand break. *Nat Struct Mol Biol* **21**:103–109.
1135 doi:10.1038/nsmb.2737
1136 55. Lee SE, Pellicioli A, Vaze MB, Sugawara N, Malkova A, Foiani M, Haber JE. 2003. Yeast
1137 Rad52 and Rad51 Recombination Proteins Define a Second Pathway of DNA Damage
1138 Assessment in Response to a Single Double-Strand Break. *Mol Cell Biol* **23**:8913–8923.
1139 doi:10.1128/mcb.23.23.8913-8923.2003
1140 56. Lim G, Chang Y, Huh W-K. 2020. Phosphoregulation of Rad51/Rad52 by CDK1 functions
1141 as a molecular switch for cell cycle-specific activation of homologous recombination. *Sci*
1142 *Adv* **6**.
1143 57. Lisby M, Mortensen UH, Rothstein R. 2003. Colocalization of multiple DNA double-strand
1144 breaks at a single Rad52 repair centre, NATURE CELL BIOLOGY.
1145 58. Lisby M, Rothstein R, Mortensen UH. 2001. Rad52 forms DNA repair and recombination
1146 centers during S phase. *Proc Natl Acad Sci U S A* **98**:8276–8282.
1147 doi:10.1073/PNAS.121006298/ASSET/55754FA8-24FB-44C3-8D0D-
1148 05A332BD04A3/ASSETS/GRAPHIC/PQ1210062005.JPEG
1149 59. Longtine MS, Mckenzie III A, Demarini DJ, Shah NG, Wach A, Brachat A, Philippsen P,
1150 Pringle JR. 1998. Additional modules for versatile and economical PCR-based gene

1151 deletion and modification in Saccharomyces cerevisiae. *Yeast* **14**:953–961.
1152 doi:10.1002/(SICI)1097-0061(199807)14:10<953::AID-YEA293>3.0.CO;2-U
1153 60. Lowndes NF, Toh GWL. 2005. DNA repair: The importance of phosphorylating histone
1154 H2AX. *Current Biology* **15**:R99–R102. doi:10.1016/j.cub.2005.01.029
1155 61. Luconi L, Araki Y, Erlemann S, Schiebel E. 2011. The CENP-A chaperone Scm3 becomes
1156 enriched at kinetochores in anaphase independently of CENP-A incorporation. *Cell Cycle*
1157 **10**:3369–3378. doi:10.4161/CC.10.19.17663
1158 62. Luo D, Liao S, Liu Y, Lin Y, Li Y, Liao X. 2022. Holliday Cross-Recognition Protein HJURP:
1159 Association With the Tumor Microenvironment in Hepatocellular Carcinoma and With
1160 Patient Prognosis. *Pathology and Oncology Research* **28**.
1161 doi:10.3389/PORE.2022.1610506
1162 63. Ma C-H, Kumar D, Jayaram M, Ghosh SK, Iyer VR. 2023. The selfish yeast plasmid
1163 exploits a SWI/SNF-type chromatin remodeling complex for hitchhiking on chromosomes
1164 and ensuring high-fidelity propagation. *PLoS Genet* **19**:e1010986.
1165 doi:10.1371/journal.pgen.1010986
1166 64. MacGilvray ME, Shishkova E, Place M, Wagner ER, Coon JJ, Gasch AP. 2020. The
1167 phosphoproteome response to dithiothreitol reveals unique versus shared features of
1168 Saccharomyces cerevisiae stress responses. *J Proteome Res* **19**:3405.
1169 doi:10.1021/ACS.JPROTEOME.0C00253
1170 65. Makrantoni V, Robertson D, Marston AL. 2019. Analysis of the Chromosomal Localization
1171 of Yeast SMC Complexes by Chromatin Immunoprecipitation. pp. 119–138.
1172 doi:10.1007/978-1-4939-9520-2_10
1173 66. Mandemaker IK, Fessler E, Corujo D, Kotthoff C, Wegerer A, Rouillon C, Buschbeck M,
1174 Jae LT, Mattiroli F, Ladurner AG. 2023. The histone chaperone ANP32B regulates
1175 chromatin incorporation of the atypical human histone variant macroH2A. *Cell Rep*
1176 **42**:113300. doi:10.1016/j.celrep.2023.113300
1177 67. McKinley KL, Cheeseman IM. 2016. The molecular basis for centromere identity and
1178 function. *Nat Rev Mol Cell Biol* **17**:16–29. doi:10.1038/NRM.2015.5
1179 68. Mehta, G. D., Agarwal, M., & Ghosh, S. K. (2014). Functional characterization of
1180 kinetochore protein, Ctf19 in meiosis I: an implication of differential impact of Ctf19 on the
1181 assembly of mitotic and meiotic kinetochores in Saccharomyces cerevisiae. *Molecular*
1182 *Microbiology*, *91*(6), 1179–1199. https://doi.org/10.1111/mmi.12527
1183 69. Melo J, Toczyski D. 2002. A unified view of the DNA-damage checkpoint. *Curr Opin Cell*
1184 *Biol*. doi:10.1016/S0955-0674(02)00312-5
1185 70. Mishra PK, Au WC, Choy JS, Kuich PH, Baker RE, Foltz DR, Basrai MA. 2011.
1186 Misregulation of Scm3p/HJURP Causes Chromosome Instability in Saccharomyces
1187 cerevisiae and Human Cells. *PLoS Genet* **7**:1002303.
1188 doi:10.1371/JOURNAL.PGEN.1002303
1189 71. Mittal P, Ghule K, Trakroo D, Prajapati HK, Ghosh SK. 2020. Meiosis-Specific Functions
1190 of Kinesin Motors in Cohesin Removal and Maintenance of Chromosome Integrity in
1191 Budding Yeast. *Mol Cell Biol* **40**. doi:10.1128/MCB.00386-19
1192 72. Miyazaki T, Bressan DA, Shinohara M, Haber JE, Shinohara A. 2004. In vivo assembly
1193 and disassembly of Rad51 and Rad52 complexes during double-strand break repair.
1194 *EMBO J* **23**:939. doi:10.1038/SJ.EMBOJ.7600091
1195 73. Mizuguchi G, Xiao H, Wisniewski J, Smith MM, Wu C. 2007. Nonhistone Scm3 and
1196 histones CenH3-H4 assemble the core of centromere-specific nucleosomes. *Cell*
1197 **129**:1153–1164. doi:10.1016/J.CELL.2007.04.026
1198 74. Montes de Oca R, Gurard-Levin ZA, Berger F, Rehman H, Martel E, Corpet A, de Koning
1199 L, Vassias I, Wilson LOW, Meseure D, Reyal F, Savignoni A, Asselain B, Sastre-Garau X,
1200 Almouzni G. 2015. The histone chaperone HJURP is a new independent prognostic
1201 marker for luminal A breast carcinoma. *Mol Oncol* **9**:657–674.
1202 doi:10.1016/J.MOLONC.2014.11.002
1203 75. Müller S, MontesdeOca R, Lacoste N, Dingli F, Loew D, Almouzni G. 2014.
1204 Phosphorylation and DNA binding of HJURP determine its centromeric recruitment and

function in CenH3CENP-A loading. *Cell Rep* **8**:190–203. doi:10.1016/J.CELREP.2014.06.002

76. Nishimura, K., Fukagawa, T., Takisawa, H., Kakimoto, T., & Kanemaki, M. (2009). An auxin-based degron system for the rapid depletion of proteins in nonplant cells. Nature Methods 2009 6:12, 6(12), 917–922. https://doi.org/10.1038/nmeth.1401
77. Pellicioli A, Foiani M. 2005. Signal Transduction: How Rad53 Kinase Is Activated. *Current Biology* **15**:R769–R771. doi:10.1016/j.cub.2005.08.057
78. Pizzul P, Casari E, Gnugnoli M, Rinaldi C, Corallo F, Longhese MP. 2022. The DNA damage checkpoint: A tale from budding yeast. *Front Genet* **13**:995163. doi:10.3389/FGENE.2022.995163/BIBTEX
79. Prajapati HK, Agarwal M, Mittal P, Ghosh SK. 2018. Evidence of *Zip1* Promoting Sister Kinetochore Mono-orientation During Meiosis in Budding Yeast. *G3 Genes|Genomes|Genetics* **8**:3691–3701. doi:10.1534/g3.118.200469
80. Ransom M, Dennehey BK, Tyler JK. 2010. Chaperoning histones during DNA replication and repair. *Cell* **140**:183. doi:10.1016/J.CELL.2010.01.004
81. Robinson JT, Thorvaldsdóttir H, Winckler W, Guttman M, Lander ES, Getz G, Mesirov JP. 2011. Integrative genomics viewer. Nature Biotechnology 2011 29:1 29:24–26. doi:10.1038/nbt.1754
82. Rg Bewersdorf J, Bennett BT, Knight KL. 2006. H2AX chromatin structures and their response to DNA damage revealed by 4Pi microscopy.
83. Sanchez-Pulido L, Pidoux AL, Ponting CP, Allshire RC. 2009. Common ancestry of the CENP-A chaperones Scm3 and HJURP. *Cell* **137**:1173–1174. doi:10.1016/J.CELL.2009.06.010
84. Serra-Cardona A, Zhang Z. 2018. Replication-Coupled Nucleosome Assembly in the Passage of Epigenetic Information and Cell Identity. *Trends Biochem Sci* **43**:136–148. doi:10.1016/j.tibs.2017.12.003
85. Shah S, Mittal P, Kumar D, Mittal A, Ghosh SK. 2023. Evidence of kinesin motors involved in stable kinetochore assembly during early meiosis. *Mol Biol Cell* **34**. doi:10.1091/mbc.E22-12-0569
86. Sherman F. 2002. Getting started with yeast. pp. 3–41. doi:10.1016/S0076-6879(02)50954-X
87. Shivaraju M, Camahort R, Mattingly M, Gerton JL. 2011. Scm3 is a centromeric nucleosome assembly factor. *J Biol Chem* **286**:12016–23. doi:10.1074/jbc.M110.183640
88. Shuaib M, Ouararhni K, Dimitrov S, Hamiche A. 2010. HJURP binds CENP-A via a highly conserved N-terminal domain and mediates its deposition at centromeres. *Proc Natl Acad Sci U S A* **107**:1349–1354. doi:10.1073/PNAS.0913709107
89. Sirbu BM, Cortez D. 2013. DNA Damage Response: Three Levels of DNA Repair Regulation. *Cold Spring Harb Perspect Biol* **5**. doi:10.1101/CSHPERSPECT.A012724
90. Smith JS. 2022. The long and short of rDNA and yeast replicative aging. doi:10.1073/pnas.2119593119
91. Smith MM. 2002. Centromeres and variant histones: what, where, when and why? *Curr Opin Cell Biol* **14**:279–285. doi:10.1016/S0955-0674(02)00331-9
92. Stoler S, Keith KC, Curnick KE, Fitzgerald-Hayes M. 1995. A mutation in CSE4, an essential gene encoding a novel chromatin-associated protein in yeast, causes chromosome nondisjunction and cell cycle arrest at mitosis. *Genes Dev* **9**:573–586. doi:10.1101/gad.9.5.573
93. Stoler S, Rogers K, Weitze S, Morey L, Fitzgerald-Hayes M, Baker RE. 2007. Scm3, an essential Saccharomyces cerevisiae centromere protein required for G2/M progression and Cse4 localization. *Proc Natl Acad Sci U S A* **104**:10571–10576. doi:10.1073/PNAS.0703178104
94. Sun Z, Bernstein E. 2019. Histone variant macroH2A: from chromatin deposition to molecular function. *Essays Biochem* **63**:59–74. doi:10.1042/EBC20180062
95. Valente V, Serafim RB, de Oliveira LC, Adorni FS, Torrieri R, da Cunha Tirapelli DP, Espreafico EM, Oba-Shinjo SM, Marie SKN, Paçó-Larson ML, Carlotti CG. 2013.

Modulation of HJURP (Holliday Junction-Recognizing Protein) levels is correlated with glioblastoma cells survival. *PLoS One* **8**. doi:10.1371/JOURNAL.PONE.0062200

96. Valente V, Teixeira SA, Neder L, Okamoto OK, Oba-Shinjo SM, Marie SKN, Scrideli CA, Paçó-Larson ML, Carlotti CG. 2009. Selection of suitable housekeeping genes for expression analysis in glioblastoma using quantitative RT-PCR. *BMC Mol Biol* **10**:1–11. doi:10.1186/1471-2199-10-17/TABLES/5
97. Van Hooser AA, Ouspenski II, Gregson HC, Starr DA, Yen TJ, Goldberg ML, Yokomori K, Earnshaw WC, Sullivan KF, Brinkley BR. 2001. Specification of kinetochore-forming chromatin by the histone H3 variant CENP-A. *J Cell Sci* **114**:3529–3542. doi:10.1242/jcs.114.19.3529
98. Wach A. 1996. PCR-synthesis of marker cassettes with long flanking homology regions for gene disruptions in S. cerevisiae. *Yeast* **12**:259–265. doi:10.1002/(SICI)1097-0061(19960315)12:3<259::AID-YEA901>3.0.CO;2-C
99. Wang C jing, Li X, Shi P, Ding H yan, Liu Y ping, Li T, Lin P ping, Wang Y shan, Zhang G qing, Cao Y. 2020. Holliday junction recognition protein promotes pancreatic cancer growth and metastasis via modulation of the MDM2/p53 signaling. *Cell Death Dis* **11**. doi:10.1038/s41419-020-2595-9
100. Wisniewski J, Hajj B, Chen J, Mizuguchi G, Xiao H, Wei D, Dahan M, Wu C. 2014. Imaging the fate of histone Cse4 reveals de novo replacement in S phase and subsequent stable residence at centromeres. *Elife* **2014**. doi:10.7554/ELIFE.02203\
101. Xiao H, Mizuguchi G, Wisniewski J, Huang Y, Wei D, Wu C. 2011. Nonhistone Scm3 Binds to AT-Rich DNA to Organize Atypical Centromeric Nucleosome of Budding Yeast. *Mol Cell* **43**:369–380. doi:10.1016/j.molcel.2011.07.009
102. Xiao H, Wang F, Wisniewski J, Shaytan AK, Ghirlando R, Fitzgerald PC, Huang Y, Wei D, Li S, Landsman D, Panchenko AR, Wu C. 2017. Molecular basis of CENP-C association with the CENP-A nucleosome at yeast centromeres. *Genes Dev* **31**:1958–1972. doi:10.1101/GAD.304782.117/-/DC1
103. Zhao X, Chabes A, Domkin V, Thelander L, Rothstein R. 2001. The ribonucleotide reductase inhibitor Sml1 is a new target of the Mec1/Rad53 kinase cascade during growth and in response to DNA damage. *EMBO J* **20**:3544. doi:10.1093/EMBOJ/20.13.3544
104. Zhao X, Muller EGD, Rothstein R. 1998. A Suppressor of Two Essential Checkpoint Genes Identifies a Novel Protein that Negatively Affects dNTP Pools. *Mol Cell* **2**:329–340. doi:10.1016/S1097-2765(00)80277-4
105. Zhou BBS, Elledge SJ. 2000. The DNA damage response: putting checkpoints in perspective. *Nature* **408**:433–439. doi:10.1038/35044005
106. Zhou X, Li W, Liu Y, Amon A. 2021. Cross-compartment signal propagation in the mitotic exit network. *Elife* **10**. doi:10.7554/eLife.63645
107. Zinchuk V, Grossenbacher-Zinchuk O. 2014. Quantitative Colocalization Analysis of Fluorescence Microscopy Images. *Curr Protoc Cell Biol* **62**. doi:10.1002/0471143030.cb0419s62